

Orchid: Image Latent Diffusion for Joint Appearance and Geometry Generation

Akshay Krishnan^{1,2} Xinchun Yan¹ Vincent Casser³ Abhijit Kundu¹
¹Google DeepMind ²Georgia Institute of Technology ³Waymo

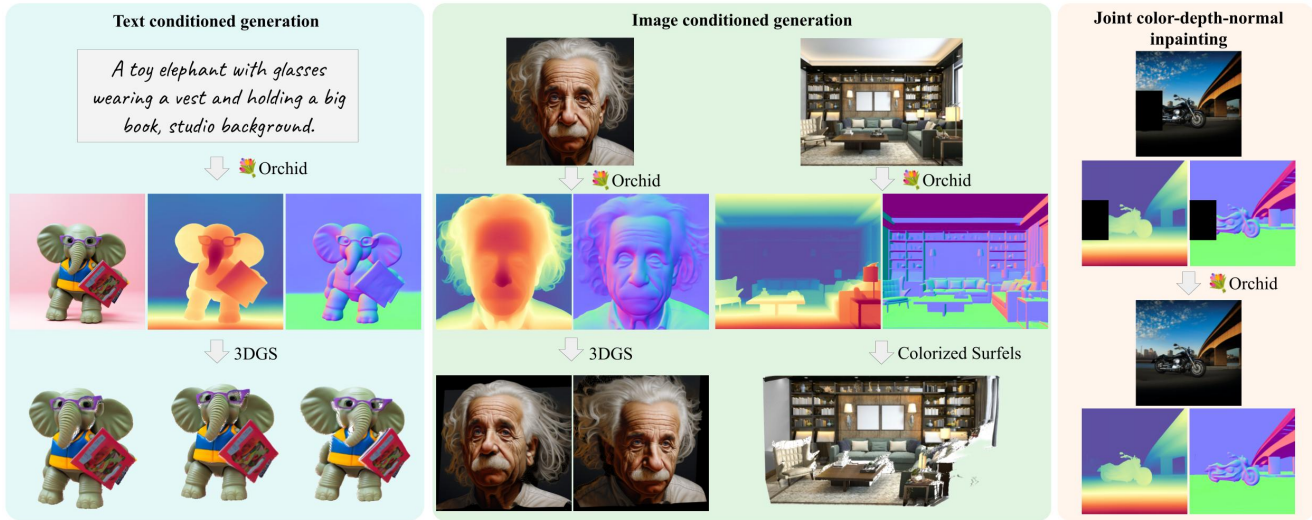


Figure 1. We propose Orchid: a unified, multi-modal latent diffusion model that jointly generates color, depth, and surface normals. The output color, depth, and normals are consistent with each other and can be seamlessly turned to 3D reconstructions using methods like 3DGS [26]. Orchid can generate 3D scenes from text (*left*), or from a single color image (*center*). Orchid captures joint appearance and geometry prior which can be used to solve different 3D inverse problems *e.g.* inpaint incomplete 2.5D reconstructions (*right*).

Abstract

Diffusion models are state-of-the-art for image generation. Trained on large datasets, they capture expressive image priors that have been used for tasks like inpainting, depth, and (surface) normal prediction. However, these models are typically trained for one specific task, *e.g.*, a separate model for each of color, depth, and normal prediction. Such models do not leverage the intrinsic correlation between appearance and geometry, often leading to inconsistent predictions.

In this paper, we propose using a novel image diffusion prior that jointly encodes appearance and geometry. We introduce a diffusion model Orchid, comprising a Variational Autoencoder (VAE) to encode color, depth, and surface normals to a latent space, and a Latent Diffusion Model (LDM) for generating these joint latents. Orchid directly generates photo-realistic color images, relative depth, and surface normals from user-provided text, and can be used to seamlessly create image aligned partial 3D scenes. It can

also perform image-conditioned tasks like monocular depth and normal prediction jointly and is competitive in accuracy to state-of-the-art methods designed for those tasks alone. Lastly, our model learns a joint prior that can be used zero-shot as a regularizer for many inverse problems that entangle appearance and geometry. For example, we demonstrate its effectiveness in color-depth-normal inpainting, showcasing its applicability to problems in sparse-view 3D generation. See orchid3d.github.io for more results.

1. Introduction

Generative 3D scene modeling [17, 21, 47, 52] has been a longstanding challenge in the computer vision and robotics community for decades. In particular, generating the appearance and geometry of 3D scenes has important applications in virtual reality [46, 51], animation [44], and robotics [1, 5, 14]. Since the scale of available 3D data is small, 3D generation models rely on priors learned from large scale 2D (color) images. In recent years, diffusion models trained on billions of color images have been




	Diff + FF	Diff + Diff	Joint Diff
# Independent models	3	3	1
Inference speed	 (mid)	 (slow)	 (fast)
Geometry generative prior	✗	✓	✓
Joint image-geometry prior	✗	✗	✓
Consistent depth-normal	✗	✗	✓

Table 1. **Comparison of methodologies for 2.5D/3D generation:** *Diff + FF* diffuses color image followed by feedforward models for depth + normal prediction; *Diff + Diff* diffuses images, then diffuses depth and normal conditioned on the color image; *Joint Diff* (Orchid) jointly diffuses color, depth and normal.

adopted as an appearance prior for generating 3D objects or scenes. A typical 3D scene generation workflow involves using a standard image diffusion model for appearance followed by separate models each for depth and surface normal estimation (e.g., DepthAnythingV2 [60], Marigold [25], Lotus-G [18], and DSINE [2]). However, the appearance and geometry of 3D scenes are tightly coupled by nature. In this paper, we introduce a joint generative model of appearance and geometry for 3D scene generation.

We propose a new method, *Orchid*, for the *joint* diffusion of appearance and geometry in a unified image latent space. Leveraging 2D priors from large-scale pre-training on color images, we propose a new *joint* latent space that extends the image diffusion latent space to incorporate 3D priors in the form of depth and surface normals. Specifically, we train a Variational Autoencoder (VAE) by taking depth and normal as extra input and output channels, initialized with a pre-trained color space VAE learned from billions of color images. Such training enables us to jointly encode and decode image, depth, and normal using a single model. Given the joint latent space as constructed by our VAE, we further train a latent diffusion model (LDM) to denoise the joint latents on a large dataset. Specifically, we craft a dataset containing coupled color, depth, and normal in a similar fashion as [59, 60] for joint modeling. Our learned joint diffusion priors can be used to directly generate color, depth and surface normals from input text prompts. The same priors can be further used to jointly generate depth and surface normals from input color images by finetuning as a color-conditioned model without text prompts.

A joint prior has several advantages over a combination of an color image prior and color-conditioned downstream models for depth or normal, as summarized in Table 1. It is faster as it only needs a single model. By directly sampling from the joint distribution, it also avoids the compounding error problem of stacking specialized models (performing depth/normal estimation based on generated color output) and the inherent information loss between the models which can cause ambiguity and estimation errors. But most importantly, we found that depth and normal predictions from

Orchid are more consistent with each other than depth and normal produced by separate models.

In addition to the above advantages for geometry generation, our joint diffusion model is a 2.5D foundation model that can be used for various applications. We demonstrate that it can be used as an color-conditioned depth and normal prediction model. Incorporating color, depth and normal into a shared latent space also allows us to perform multi-modal inpainting: joint generation of all modalities using a partial subset of observations. Orchid has several potential applications in robotics and virtual reality, including depth completion from color image and sparse LiDAR depth, inpainting holes produced during novel view synthesis from sparse views, and interactive 3D experience. It could also be used in a score-distillation framework, providing a depth and normal aware score function.

In summary, our contributions are as follows:

- We introduce Orchid, a single joint diffusion model to generate both appearance and geometry. Key to our method is a new *joint* latent space that extends the image diffusion latent space to incorporate depth and normals.
- We train Orchid’s VAE with extra input and output channels to learn a joint latent space from a large dataset with paired color, depth, and normals. When trained on the new joint latent space, Orchid can accurately generate appearance and geometry jointly from input text prompts.
- Orchid serves as a foundation model for various downstream applications, including monocular depth and normal prediction (with finetuning) and zero-shot multi-modal inpainting. Orchid’s monocular depth and normal predictions are competitive with SOTA methods that use separate models, while being more consistent.

2. Related work

Monocular depth and normal prediction: *Monocular depth estimation* is an extensively studied problem in computer vision. Modern deep depth prediction models rely on priors learned from large scale datasets [3, 11–13, 22, 25, 30, 39, 59, 60]. Since metric depth is a function of the camera’s intrinsics parameters, most approaches predict affine-invariant depth. Models that predict metric depth either predict depth for a single camera [11] or condition on the camera intrinsics [3, 16, 22]. However, since the amount of depth data with known camera intrinsics is limited, most recent methods with zero-shot generalization capabilities, much like our model, predict affine-invariant relative depth.

Monocular surface normal prediction has also seen similar trends as depth prediction, with training deep models for feed-forward prediction being the standard approach [9, 54]. In particular, [9] achieved state-of-the-art performance following this setup. The most recent state-of-the-art [2] incorporates inductive biases specific to the normal prediction task into the deep model.

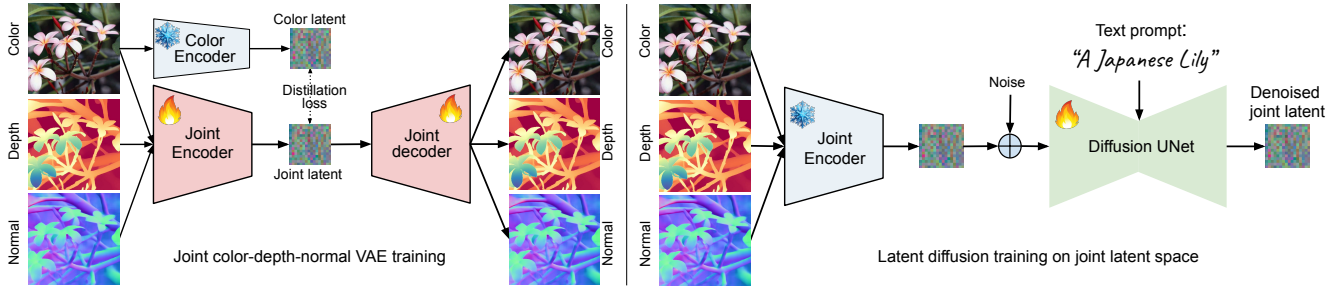


Figure 2. **Orchid training architecture:** As illustrated on the left figure, we first train a joint color-depth-normal VAE that leverages priors from color-only pretraining. We introduce additional depth and normal reconstruction losses, along with a distillation loss to ensure that the joint latent space follows the structure of the original color-only VAE. As illustrated on the right figure, we then train the latent diffusion model on paired image-depth-normal and text data, while keeping the joint VAE encoder frozen.

Joint prediction of depth and surface normals has been explored by a few works as a multi-task problem. They are modelled using two branches on a deep network with a shared backbone [10, 29, 57, 63].

Most recent approaches for depth [59, 60] and normal prediction [22] adopt self-supervised ViT backbones [37], and train jointly on several large datasets to achieve zero-shot in-the-wild generalization. Although they can predict depth and normals from images, they are discriminative and do not learn a generative prior that can be leveraged for tasks like depth completion.

Diffusion priors for depth and normals: Several recent works [8, 13, 24, 25, 48, 49] have shown that diffusion priors learned from large color image datasets can be adapted for depth and normal estimation by finetuning them on relatively small amounts of data. These color-conditioned depth and normal diffusion models learn a generative 2D prior of depth which can be used for tasks like depth completion.

However, when used to generate 3D scenes, they impose a two-step process where a color image is first generated using a diffusion model, followed by depth and/or normal generation using another diffusion model. In contrast, our model learns a joint prior over color, depth and normal.

Diffusion priors for inverse problems: The 2D priors learned by text-to-color diffusion models have been leveraged for controlled generation tasks such as inpainting or super-resolution. The two main approaches to use diffusion priors either 1) train a masked image conditioned model [61] model on additional data [56], or 2) use the conditioning image to guide the diffusion process without additional training [6, 35, 42, 43]. The second approach is more appealing since it does not require additional training and retains the diffusion model’s generalization capabilities. We use this approach with our learned diffusion prior to jointly inpaint color, depth and normals.

The diffusion image priors have also been used for 3D scene generation conditioned on text or single-view color image. One family of approaches uses diffusion models as

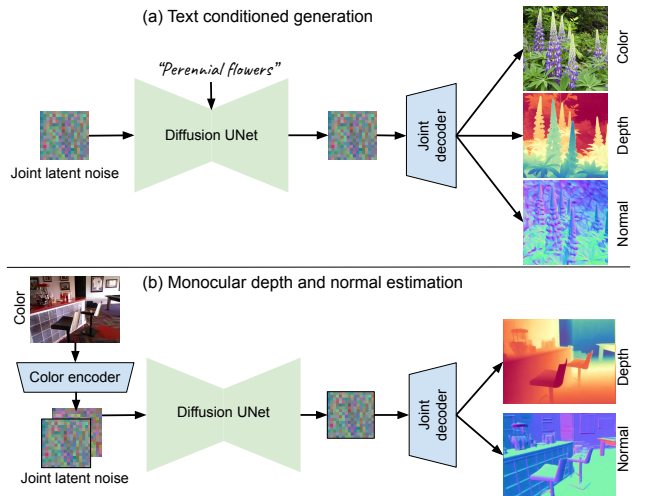


Figure 3. **Orchid inference:** (a) For text-conditioned generation, We denoise the joint latents conditioned on the text prompt; (b) For monocular depth / normal estimation, we denoise the joint latents with a noise-free latent of the input color image as condition.

novel view priors within an optimization framework using a variant of the score-distillation loss [32, 34, 38, 55, 58]. We believe such work can benefit from a joint appearance-geometry prior that avoids the need for cascaded methods and provides score functions that capture the joint appearance-geometry likelihood.

3. Method

Orchid is a latent diffusion model that learns a joint 2D generative prior of appearance (RGB) and 3D geometry (depth and surface normals). More specifically, it learns a score function for the joint distribution $p(\mathbf{x}, \mathbf{d}, \mathbf{n} | \mathcal{T})$ of color $\mathbf{x} \in \mathbb{R}^{H \times W \times 3}$, depth $\mathbf{d} \in \mathbb{R}^{H \times W}$, and surface normals $\mathbf{n} \in [-1, 1]^{H \times W \times 3}$ (with $\|\mathbf{n}\|_2 = 1$), conditioned on text prompts \mathcal{T} . This is a foundational generative prior that can be used for various tasks, such as text-conditioned appearance and geometry generation (sampling

from $p(\mathbf{x}, \mathbf{d}, \mathbf{n}|\mathcal{T})$, color-conditioned depth and normal estimation (sampling from $p(\mathbf{d}, \mathbf{n}|\mathbf{x})$), and joint multi-modal inpainting.

Central to our method is (1) a joint latent space VAE (Section 3.1) that additionally encodes and decodes depth and normals, building upon 2D priors learned by color-space VAE; and (2) a joint diffusion prior (Section 3.2) with the ability to generate depth and normals in addition to color. The generative priors learn by Orchid can be used for color-conditioned depth and normal prediction by fine-tuning on an added color image condition (Section 3.3).

3.1. Joint latent space VAE

The conventional color-space VAE encoder [27, 41] projects pixels to a compact latent space, which diffusion models use for generation by iterative denoising. To jointly model appearance and geometry, we extend the conventional VAE to include depth and normals by adding four more input and output channels (one for depth and three for normals). This design allows Orchid to decode all three modalities jointly at once, without relying on separate models (e.g., monocular depth estimators) to predict geometry. Using a joint VAE for appearance and geometry also allows the encoder to learn a unified compact latent space, minimizing redundancies in depth and normal representations. This is unlike other diffusion-based depth models that duplicate depth across 3 channels to reuse the VAE [13, 18, 25].

We preprocess depth before it is input to the VAE. In particular, from metric depth \mathbf{d} , we compute inverse depth $\mathbf{d}^* = 1/\mathbf{d}$, and its mean deviation around the median: $d_\sigma = \text{mean}(|\mathbf{d}^* - \text{median}(\mathbf{d}^*)|)$. We normalize inverse depth by the deviation $\mathbf{d}' = \mathbf{d}^*/d_\sigma$. We then shift it to begin at zero: $\mathbf{d}_{\text{model}} = \mathbf{d}' - d'_{\text{min}}$. To simplify notation, we use \mathbf{d} to denote the preprocessed depth $\mathbf{d}_{\text{model}}$.

We fine-tune our joint VAE on paired color, depth, and normal datasets. We apply various losses ($L_{\mathbf{x}}$, $L_{\mathbf{d}}$, $L_{\mathbf{n}}$) for joint color, depth, and normal supervision, including a shared KL regularization loss L_{KL} and a distillation loss L_{distill} on the joint latent space. We find the distillation loss crucial to encourage our VAE’s latents to be close in distribution to the color VAE, to retain diffusion priors from color pretraining (Section 4.5). We supervise our color predictions using reconstruction loss $L_{\text{rec}} = \|\hat{\mathbf{x}} - \mathbf{x}\|_2$, adversarial loss L_{adv} , perceptual loss $L_{\text{LPIPS}} = \|\mathcal{F}_{\text{VGG}}(\hat{\mathbf{x}}) - \mathcal{F}_{\text{VGG}}(\mathbf{x})\|_2$ (see [62]), and locally-discriminative learning loss $L_{\text{local_disc}}$ [31]. These losses follow the standard practices from conventional color-space VAE literature [41].

We supervise our depth and normal prediction using depth reconstruction loss $L_{\text{depth_rec}} = \|\hat{\mathbf{d}} - \mathbf{d}\|_1$, the multi-scale scale-invariant depth gradient loss $L_{\text{depth_grad}}$ [30], and the normal reconstruction loss $L_{\text{normal_rec}} = \|\hat{\mathbf{n}} - \mathbf{n}\|_2$. The full training loop is summarized in Alg. 1. We further use an exponential moving average for updating the VAE encoder

and decoder parameters.

$$\begin{aligned} L_{\mathbf{x}} &= w_1^{\mathbf{x}} L_{\text{rec}} + w_2^{\mathbf{x}} L_{\text{adv}} + w_3^{\mathbf{x}} L_{\text{LPIPS}} + w_4^{\mathbf{x}} L_{\text{local_disc}} \\ L_{\mathbf{d}} &= w_1^{\mathbf{d}} L_{\text{depth_rec}} + w_2^{\mathbf{d}} L_{\text{depth_grad}} \\ L_{\mathbf{n}} &= w^{\mathbf{n}} L_{\text{normal_rec}} \end{aligned}$$

Algorithm 1 Joint VAE training

```

Initialize model weights  $\theta = [\theta_{\text{enc}}, \theta_{\text{dec}}, \theta_{\text{disc}}]$ 
for  $i = 1, \dots, \text{num\_steps}$  do
    Sample coupled color  $\mathbf{x}$ , depth  $\mathbf{d}$ , normal  $\mathbf{n}$ 
     $[\mathbf{z}_\mu, \mathbf{z}_\sigma] \leftarrow \text{Enc}(\mathbf{x}, \mathbf{d}, \mathbf{n}; \theta_{\text{enc}})$ 
     $\mathbf{z}_{\text{sample}} \leftarrow \mathcal{N}(\mathbf{z}_\mu, \mathbf{z}_\sigma)$ 
     $L_{\text{KL}} \leftarrow w^{\text{KL}} * \text{KL}(\mathcal{N}(\mathbf{z}_\mu, \mathbf{z}_\sigma) \parallel \mathcal{N}(\mathbf{0}, \Sigma))$ 
     $[\hat{\mathbf{x}}, \hat{\mathbf{d}}, \hat{\mathbf{n}}] \leftarrow \text{Dec}(\mathbf{z}_{\text{sample}}; \theta_{\text{dec}})$ 
     $L_{\text{disc}} \leftarrow \log(\text{Disc}(\mathbf{x}; \theta_{\text{disc}})) + \log(1 - \text{Disc}(\hat{\mathbf{x}}; \theta_{\text{disc}}))$ 
    Update parameters according to gradients
     $\theta_{\text{enc}} \stackrel{\pm}{\leftarrow} -\nabla_{\theta_{\text{enc}}} (L_{\mathbf{x}} + L_{\mathbf{d}} + L_{\mathbf{n}} + \alpha L_{\text{KL}} + \beta L_{\text{distill}})$ 
     $\theta_{\text{dec}} \stackrel{\pm}{\leftarrow} -\nabla_{\theta_{\text{dec}}} (L_{\mathbf{x}} + L_{\mathbf{d}} + L_{\mathbf{n}} - \gamma L_{\text{disc}})$ 
     $\theta_{\text{disc}} \stackrel{\pm}{\leftarrow} -\nabla_{\theta_{\text{disc}}} L_{\text{disc}}$ 
end for

```

3.2. Joint diffusion prior for color-depth-normal

We train a latent diffusion model (LDM) to jointly denoise color-depth-normal latents \mathbf{z} . In the forward process, we inject noise in the joint latent space through $\mathbf{z}_t = \sqrt{\alpha_t} \mathbf{z}_0 + \epsilon \sqrt{1 - \alpha_t}$ and $\epsilon \sim \mathcal{N}(0, \mathbf{I})$ by following $q(\mathbf{z}_t | \mathbf{z}_0) = \mathcal{N}(\mathbf{z}_t; \sqrt{\alpha_t} \mathbf{z}_0, (1 - \alpha_t) \mathbf{I})$. Here, \mathbf{z}_t represents the noisy input at diffusion time t and $\alpha_t = \prod_{s=1}^t (1 - \beta_s)$ is the diffusion coefficient [20]. In the *reverse* process, our latent diffusion model (parameterized by θ_{LDM}) predicts the target y given \mathbf{z}_t and diffusion time t . We optimize the standard objective function $L_{\text{LDM}} = \mathbb{E}_{\epsilon \in \mathcal{N}(0, \mathbf{I}), t \in \mathcal{U}(T)} [\|y - f_{\theta_{\text{LDM}}}(\mathbf{z}_t, t)\|^2]$. We use the v -prediction (velocity) parametrization for our target y [45]. We train our LDM to denoise joint latents conditioned on text embeddings (Figure 2). This allows us to directly use Orchid to generate color, depth and surface normals from text prompts with classifier-free guidance [19] (Figure 3a).

3.3. Color-conditioned depth and normal prediction

The formulation in Section 3.2 allows us to generate color, depth, and normals directly from the joint latent space through $f_{\theta_{\text{LDM}}}(\mathbf{z}_t, t)$. To further use Orchid to generate depth and surface normals jointly from an input image condition, we append an input image latent $\mathbf{z}^{\mathbf{x}}$ from the pre-trained frozen color-only VAE as a condition signal for diffusion training through $f_{\theta_{\text{LDM}}}(\mathbf{z}_t, t; \mathbf{z}^{\mathbf{x}})$. While this is in line with previous work on using diffusion priors for dense prediction [18, 25], our joint latent space allows direct generation of *both depth and surface normals* from image con-

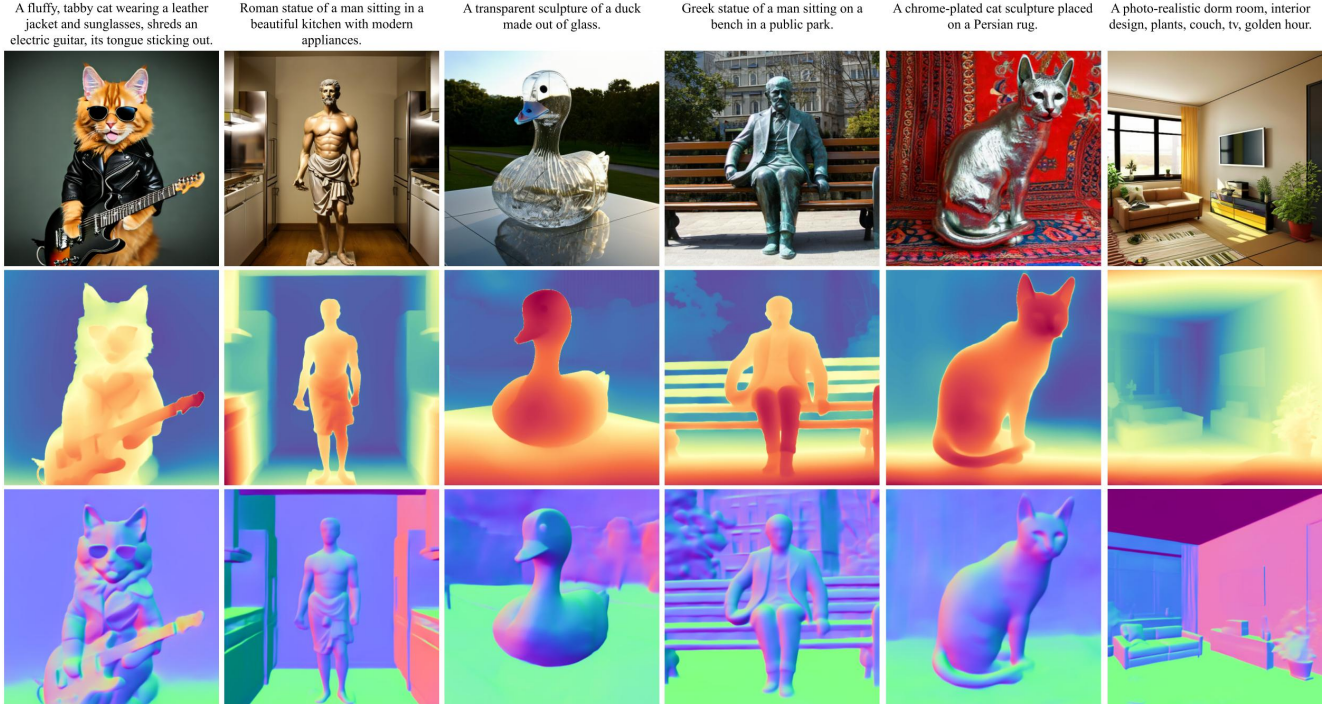


Figure 4. **Text-conditioned generation:** Color, depth and normal images generated jointly by our model from a single text prompt. The input text prompt is provided on the top. The generated color, depth, and normal are presented from top to bottom. Results show that Orchid can produce consistent appearance and geometry for a wide range of text prompts such as close-up object shots or views from complex layouts of indoor and outdoor environment.

ditions. When used as an image-conditioned geometry estimator at inference, we drop text conditions (Figure 3b). The sampling procedure is detailed in Alg. 2.

Algorithm 2 Color-conditioned depth sampling

Require: \mathbf{z}^x (color-space latent condition), T (total denoising steps)
Initialize joint latent $\mathbf{z}_T \sim \mathcal{N}(\mathbf{0}, \mathbf{I})$
for $t = T, \dots, 1$ **do**
 $\eta \sim \mathcal{N}(\mathbf{0}, \mathbf{I})$ if $t > 1$, else $\eta = \mathbf{0}$
 $\mathbf{z}_{t-1} = \frac{1}{\sqrt{\alpha_t}} \left(\mathbf{z}_t - \frac{\beta_t}{\sqrt{1-\alpha_t}} f_{\theta_{\text{LDM}}}(\mathbf{z}_t, t; \mathbf{z}^x) \right) + \sigma_t \eta$
end for
return \mathbf{z}_0

4. Experiments

Orchid learns a joint color, depth, and surface normal prior that can be leveraged for several tasks. In our experiments, we evaluate its performance on three different tasks: text-conditioned color-depth-normal generation, color-conditioned depth and normal prediction, and unconditional joint color-depth-normal inpainting. Our experiments highlight the versatility of Orchid, showing how a joint appearance and geometry prior can be used for either text or color conditioned generation, or as an unconditional

model for solving inverse problems that combine appearance and geometry.

4.1. Implementation details

We use a convolutional encoder and decoder with a latent channel of 8 for our joint VAE, initialized from a VAE pretrained on datasets of color images alone. For the latent diffusion model, we use a transformer UNet similar to Stable Diffusion [41] pretrained on a large image-text dataset. The diffusion model uses v -prediction. We train both models on 512x512 image resolution. When training our text and color-conditioned diffusion models, we use a DDPM noise schedule [20] with 1000 steps. For diffusion sampling, we adopt a DDIM schedule with 100 steps for text-conditioned generation and 50 steps for image-conditioned generation. We use the zero terminal SNR schedule from [33].

Dataset: We combine many real and synthetic datasets with ground truth depth and surface normals to train our VAE: Omnidata [9], Virtual KITTI [14], Hypersim [40], and DIODE [53]. Additionally, we create a large-scale dataset with text, color, depth and normals by using large pretrained models to predict depth [60] and surface normal [22] from a text-image dataset. We use approximately 2.5M images with ground truth depth and surface normal, and about 100M images with pseudo ground truth.

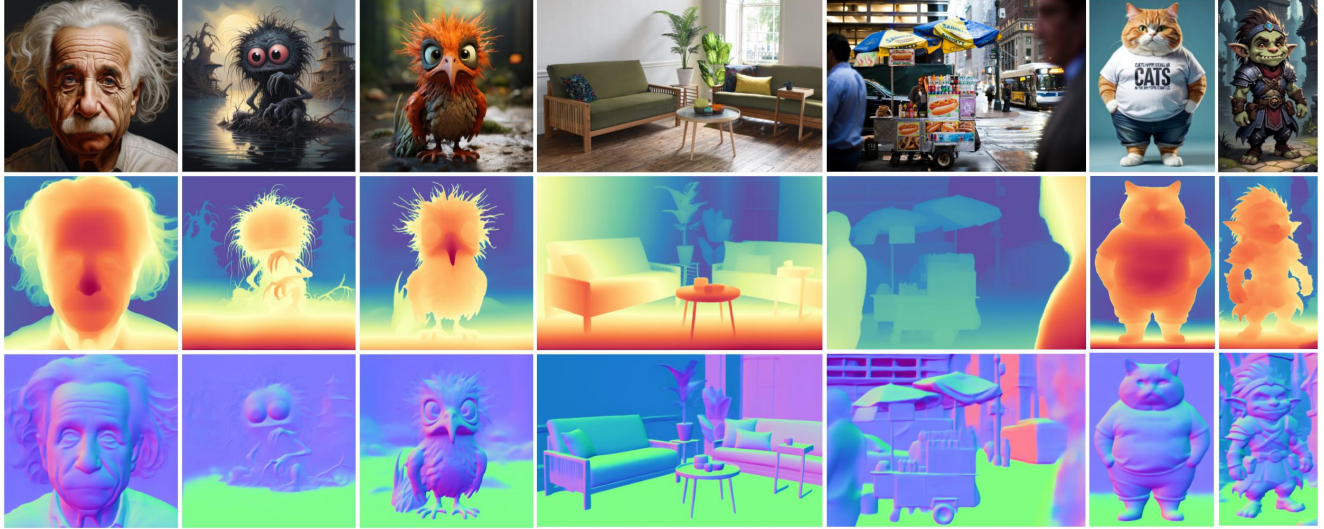


Figure 5. **Joint depth and surface normal prediction from single color image:** Given in-the-wild images as input (top row), Orchid works jointly predicts accurate and consistent depth (middle row) and normal (bottom row).

4.2. Text-conditioned generation

Orchid is a first-of-its-kind model that can jointly generate color images along with their depth and normal from text prompts. We provide qualitative results of color, depth and normal generated by Orchid from a diverse set of text prompts in Figure 4. Assuming approximate intrinsics, we can use the predicted color, depth and surface normal to optimize 3D Gaussians using Gaussian Splatting [26]. We show an example of this in Figure 1. Additional results are provided in Appendix C.

4.3. Monocular depth and normal prediction

The joint color-depth-normal prior learned by Orchid can also be leveraged for monocular depth and normal prediction with color-conditioned fine-tuning (Section 3.3). We evaluate the accuracy of the depth and normal *jointly estimated* by Orchid from color images. We follow the protocol in recent approaches and evaluate the zero-shot performance on standard benchmarks we do not train on. In addition, we present qualitative results in Figure 5. As illustrated in the figure, our model can produce high-fidelity and consistent depth and normal estimation from in-the-wild color images that contain single objects, indoor, and outdoor complex scene environment.

Zero-shot monocular depth estimation: We evaluate the accuracy of the affine-invariant depth estimated by Orchid on four held-out datasets: NYUDepthv2 [36], KITTI [15], ETH3D [50] and ScanNet [7]. We compare Orchid’s performance to other zero-shot depth estimation baselines. This includes feed-forward models [22, 39, 60] as well as models that learn a conditional depth estimation prior by finetuning image generative models [13, 25]. Note

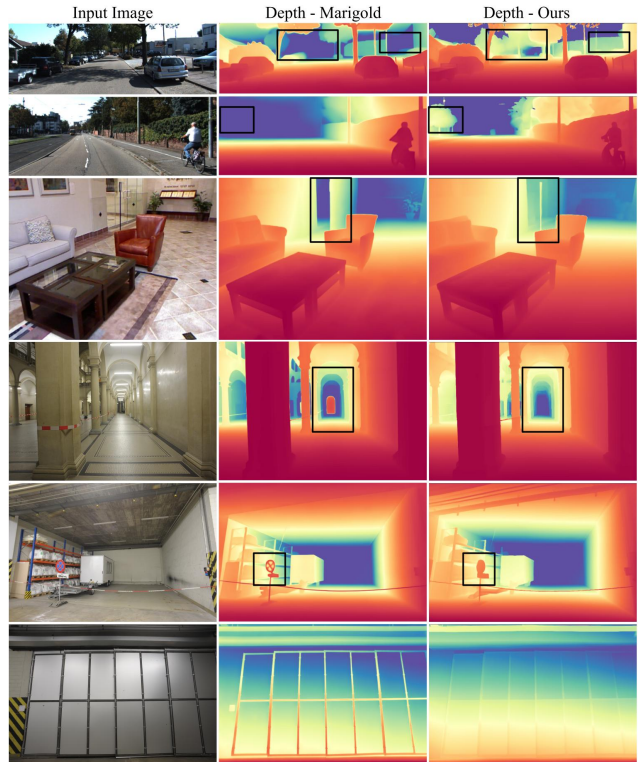


Figure 6. **Monocular depth prediction:** Orchid obtains more accurate depth compared to Marigold [25], as highlighted in the results shown above. Our model achieves better performance on far-range objects (row 1,2,4), small objects (row 5), depth-ambiguous scenes (row 6), and transparent occlusions (row 3).

that all our baselines (except [13]) are explicitly trained for color-conditioned depth prediction while Orchid jointly predicts depth and normals. As demonstrated in Table 2,

Model	NYUv2		KITTI		ETH3D		ScanNet	
	AbsRel ↓	δ_1 ↑	AbsRel ↓	δ_1 ↑	AbsRel ↓	δ_1 ↑	AbsRel ↓	δ_1 ↑
MiDaS [39]	11.7	87.5	23.6	63.0	18.4	75.2	12.1	84.6
DepthAnything v2 [60]	4.5	97.9	7.4	94.6	6.8	95.3	6.0	96.3
Marigold-depth [25]	6.1	95.8	9.8	91.8	6.8	95.6	6.9	94.6
Lotus-G-depth [18]	5.4	96.6	11.3	87.7	6.2	96.1	6.0	96.0
Geowizard [13]	5.6	96.3	14.4	82.0	6.6	95.8	6.4	95.0
Orchid (Ours)	5.7	96.9	7.7	94.4	7.3	96.9	6.3	95.8

Table 2. **Zero-shot monocular depth estimation:** Comparison of our zero shot affine-invariant depth estimation accuracy to that of other methods. Our accuracy is comparable to that of [60] while being better than the other joint depth-normal method [13]. The **first**, **second** and **third** ranking methods are highlighted.

Model	NYUv2		ScanNet		iBims-1		Sintel	
	Mean ↓	11.25° ↑	Mean ↓	11.25° ↑	Mean ↓	11.25° ↑	Mean ↓	11.25° ↑
Omnidata v2 [9]	17.2	55.5	16.2	60.2	18.2	63.9	40.5	14.7
DSINE [2]	16.4	59.6	16.2	61.0	17.1	67.4	34.9	21.5
Marigold-normal [25]	20.9	50.5	21.3	45.6	18.5	64.7	-	-
Lotus-G-normal [18]	16.9	59.1	15.3	64.0	17.5	66.1	35.2	19.9
Geowizard [13]	18.9	50.7	17.4	53.8	19.3	63.0	40.3	12.3
Orchid (Ours)	15.2	60.6	14.2	63.8	16.3	68.1	31.7	22.6

Table 3. **Zero-shot monocular surface normals estimation:** Comparison of our color-conditioned normal estimation accuracy to state-of-the-art. Orchid is significantly better than other methods while jointly predicting both depth and normals. The **first**, **second** and **third** ranking methods are highlighted.

Dataset	Marigold [25]	GeoWizard [13]	Orchid
NYUv2	0.102	0.122	0.040
KITTI	0.146	0.324	0.082

Table 4. **Depth-normal inconsistency:** We show the mean error $e_{\text{depth_normal}}$ (\downarrow) in the table. Orchid’s color-conditioned joint depth and normal estimates are significantly more consistent than those produced by GeoWizard or separate Marigold models.

Orchid’s depth estimates are comparable to the state-of-the-art method [60], while being better than other diffusion-based baselines. As illustrated in Figure 6, our method produces more accurate depth than Marigold [25] on far-range objects, small objects, and depth-ambiguous scenes. Notably, Orchid achieves better monocular depth estimation performance than Geowizard [13], the only baseline that jointly predicts depth and surface normals.

Zero-shot monocular surface normals estimation: We also evaluate Orchid’s normal estimation accuracy on four held-out datasets: NYUv2 [36], ScanNet [7], iBims-1 [28] and Sintel [4]. As shown in Table 3, Orchid is significantly better than baselines at estimating surface normal. This highlights the significance of training a VAE that explicitly encodes color, depth and normal into a joint latent on a large scale dataset, as opposed to other diffusion baselines [13, 18, 25] that use a frozen color-space VAE

to encode and decode depth and normal. We visualize the comparisons to Marigold-normal [25] in Figure 7, where our method has stronger normal prediction performances on curved and deformable surfaces.

Depth-normal consistency: We evaluate the consistency of the depth and surface normal produced by Orchid and compare it to other diffusion baselines that either use separate model weights or switch embedding to predict depth and normal [13, 25]. We align the affine-invariant depth $\hat{\mathbf{d}}$ with ground truth to get metric depth predictions \mathbf{d} , which we use with camera intrinsics to compute a 3D pointcloud \mathbf{p} . We use the pointcloud to estimate normals $\hat{\mathbf{n}} = \nabla_x \mathbf{p} \times \nabla_y \mathbf{p}$ from depth, and compute its inconsistency $e_{\text{depth_normal}} = (1 - \hat{\mathbf{n}} \cdot \mathbf{n})/2$ with the estimated normals \mathbf{n} . As shown in Table 4, we find that Orchid is able to leverage the joint latent space to predict depth and normal that are significantly more consistent. We visualize the depth-normal inconsistency error map in Figure 8. These results clearly demonstrate the benefit of our joint generative model of appearance and geometry in downstream applications.

4.4. Joint color-depth-normal inpainting

The joint color-depth-normal generative prior learned by Orchid can be used for unconditional tasks that combine appearance and geometry, such as jointly inpainting both color and geometry. Given color, depth and normals for a

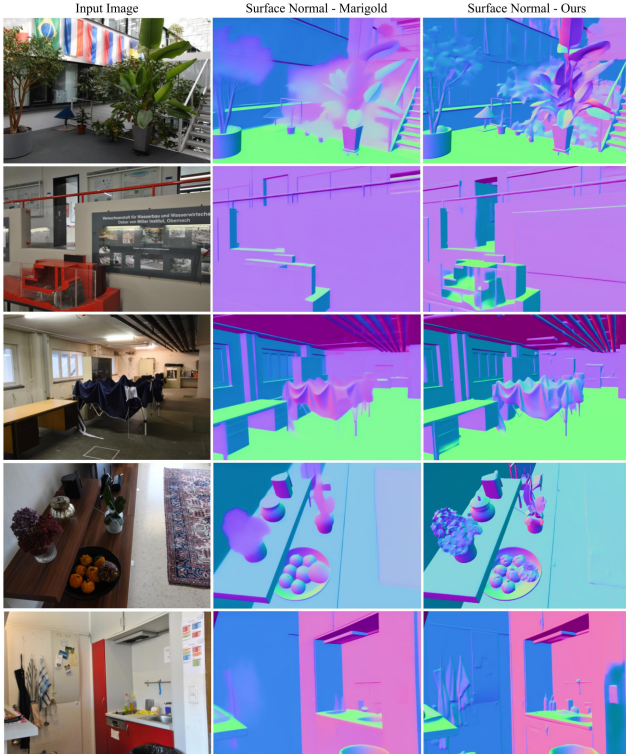


Figure 7. **Monocular surface normal prediction:** A comparison of our jointly generated normal to that of color-conditioned prediction using Marigold [25]. Orchid produces more robust results on curved and deformable surfaces.

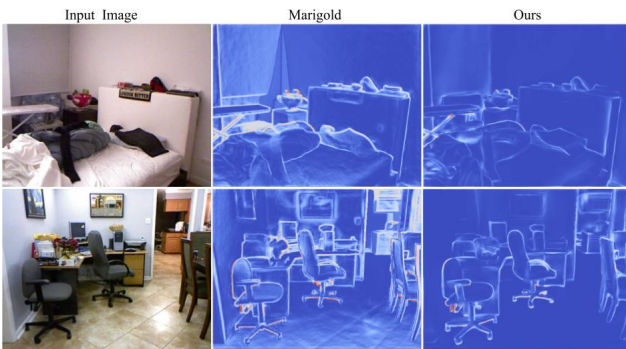


Figure 8. **Depth-normal consistency:** This heatmap of predicted depth-normal *inconsistency* shows that our joint predictions are more consistent with each other, compared to Marigold [25].

frame, we mask all of them for the region to be inpainted (input in Figure 9). Following the approach from RePaint [35], we use Orchid as an unconditional inpainting prior to generate inpainted regions, as shown in Figure 9. We find that our model is able to generate plausible inpainted regions with consistent color, depth and normals, without any additional training. This is a unique capability that results from Orchid’s joint prior. Please refer to Appendix C.4 for more inpainting results.

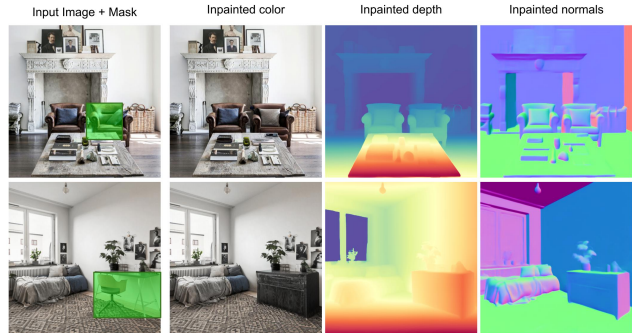


Figure 9. **Joint color-depth-normal inpainting:** Given a masked region in color-depth-normal data (left column shows masked color), our model inpaints them jointly using an approach like [35].

4.5. Ablations

We ablated the impact of some choices we make in training Orchid’s VAE and latent diffusion model. Please find additional ablations in Appendix B.

Distillation loss: We use a distillation loss to encourage our VAE’s latents to be close in distribution to the original LDM’s latents. We find that dropping the distillation loss during VAE training makes the diffusion training forget some priors learned from image pretraining, generating qualitatively worse images. We observe a reduced CLIP image-text similarity by 0.7 and increased FID by 1.7.

Use of pseudo labels: Unlike previous methods that rely solely on real or synthetic training data, we use a large text-image dataset with depth and normals from pretrained models. We find that this improves the VAE’s depth predictions by 1.3 AbsRel and normals by 7.7% ($< 11.25^\circ$ error).

5. Conclusion

In this work, we presented Orchid, a joint appearance and geometry diffusion prior that encodes color, depth, and surface normal in a unified latent space. This allows Orchid to be used for generating 3D reconstructions efficiently and seamlessly with just one model. The joint appearance and geometry prior captured in Orchid can be used for various downstream tasks. Notably, Orchid enables joint generation of images, depth, and surface normal from an given text prompt using a single model. Sampling from Orchid with a single color image as condition produces accurate and consistent depth and normals, which rival SOTA monocular depth and normal prediction models trained specifically for those tasks. It also excels in joint inpainting of color, depth, and surface normals when used as an unconditional diffusion prior, a capability that is unique to Orchid. We anticipate Orchid will pave the way for advancements in tasks like new-view synthesis from single and sparse observations, densification from sparse depth, and solving inverse problems that entangle appearance and geometry.

Orchid: Image Latent Diffusion for Joint Appearance and Geometry Generation

Appendix

In this appendix, we provide additional details on our datasets, model architecture, ablations and training methodology. We also provide additional qualitative results from Orchid for text conditioned color-depth-normal generation as well as image conditioned depth and inpainting tasks, including comparisons to more baselines. Also see the project website containing 3D reconstructions using predictions from Orchid (more details in Section C.5), and qualitative comparisons.

A. Orchid details

A.1. Architecture

For our VAE, we use a convolutional encoder and decoder with a latent dimension of 8, with $8 \times$ spatial downsampling. The VAE has 7 input channels: 3 for RGB, 1 for depth, and 3 for surface normals.

Once the VAE is trained, we keep it frozen when training the latent diffusion model. The latent diffusion model itself is a UNet transformer similar to *Stable Diffusion* which is conditioned on both time and text embeddings. It has approximately 2B parameters.

A.2. Training

We use a combination of different RGB, depth, and normal losses when training the VAE, weighted differently as explained in Section 3.1 of our paper. Here we provide the values of the weights we found to work best for our setting. For L_x , we use $w_1^x = 1, w_2^x = 0.1, w_3^x = 0.1, w_4^x = 1$. For L_d , we use $w_1^d = 1, w_2^d = 0.5$. We use $w^n = 1$ for L_n .

On 16 NVIDIA A100 GPUs, we take approximately 5 days to train the VAE, 2 days to finetune our LDM starting from a color LDM, and 8-12 hours to finetune our image-conditioned model.

A.3. Dataset

We provide details of the dataset we used for VAE and LDM training in Table 5.

Dataset	Size	Text	Depth	Normals
Hypersim	60k	✗	✓	✓
Virtual KITTI	21k	✗	✓	✗
Replica + GSO (Omnidata)	100k	✗	✓	✓
Taskonomy (Omnidata)	2M	✗	✓	✓
DIODE	25k	✗	✓	✓
Pseudo-labeled (ours)	110M	✓	✓	✓

Table 5. **Dataset details:** We use all the above datasets for training the VAE, but only the pseudo-labeled text-image dataset, Hypersim, and Replica + GSO for finetuning our LDM.

B. Additional ablations

This section provides ablations in addition to the ones provided in our paper.

Impact of pseudo labels: As explained in Section 4.5, we found that using predictions from pretrained models [22, 60] for depth and normal as pseudo-ground truth improves the depth and normal reconstruction accuracy of our joint color-depth-normal VAE. Here, we further ablate its impact on the finetuning of Orchid for image-conditioned depth and normal estimation. As shown in Table 6, we find that the monocular depth estimation accuracy of Orchid drops by 0.3 in δ_1 , while its surface normal prediction accuracy drops significantly by approximately 1° worse mean error, if the pseudo-labels were not used for finetuning.

Disentangled latent space for joint generation: Orchid uses a unified latent space for joint color-depth-normal generation. Another alternative design to enable a joint color-depth-normal latent space would be to explicitly encode all three modalities using shared/separate VAEs, and finetune the LDM to denoise a higher dimensional concatenation of all three latents. We find that while this is a feasible approach, the quality of generated images is worse than that of using a joint latent. Our hypothesis is that this is likely due to a significant mismatch in latent representations for the UNet when compared to the color image-only pretraining stage, as opposed to a joint latent space that is similar in structure to the pretrained LDM’s latent space. Quantitatively, Table 6 shows that this disentangled latents model has a lower CLIP-similarity score when evaluated on COCO captions. It does however have a lower FID and higher LPIPS, likely because it uses the same latent dimension to store color information alone. Our joint latent however is significantly better on image-conditioned prediction tasks, as it can better leverage the interdependencies between color, depth, and normals.

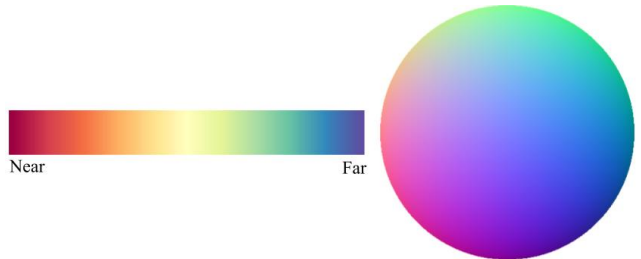


Figure 10. Colormap for depth (left) and surface normal on a unit hemisphere (right) used for all qualitative results in this paper.

Model	Text-conditioned generation			Monocular depth		Monocular normals	
	CLIP (\uparrow)	FID (\downarrow)	LPIPS (\uparrow)	AbsRel (\downarrow)	δ_1 (\uparrow)	Mean (\downarrow)	$< 11.25^\circ$ (\uparrow)
Joint latent	0.316	18.74	0.764	5.7	96.9	15.2	60.6
Distorted latents	0.312	17.11	0.769	6.4	96.0	-	-
w/o pseudo labels	-	-	-	5.7	96.6	16.12	57.9

Table 6. **Ablations:** We provide further metrics to ablate some key choices in our implementation. We find that: 1) using a joint latent instead of disentangled latents to encode color, depth and normals provides text-conditioned image generations with an improved CLIP-similarity and better image-conditioned depth and normal predictions on NYUv2; 2) using pseudo-labeled depth and surface normals on a large text-image dataset when finetuning Orchid for image-conditioned prediction degrades the depth and normal estimates significantly.

C. Qualitative results

We provide additional qualitative results and comparisons for experiments in our paper. Colormaps used to visualize the depth and surface normal predictions is shown in 10.

C.1. Note on depth map visualization

Orchid predicts affine-invariant inverse depth, unlike other baselines Marigold [25] and GeoWizard [13] that predict affine invariant depth normalized to $[0, 1]$. To compare our depth qualitatively when ground truth depth is available (Figures 14, 15, 16, 17, 18), we align all predictions to the ground truth by estimation a shift and scale offset using least squares. When ground truth is not available (Figures 12 and 13), we inverted inverse-depth produced for our method, while using the predicted depth for [25] and [13], which may appear different due to an unknown inverse-depth shift. We use the colormap in Figure 10.

C.2. Text conditioned joint generation

We show color-depth-normals generated by our model for different text prompts in Figure 11. Figure 12 compares the results from our model to a baseline that uses a color-only LDM to first generate color, and then depth and normal diffusion models to generate depth and surface normals. The results from a single pass of our model are comparable to these results. Figure 13 compares the depth and normals generated by our model to those predicted by depth and normal prediction baselines on our images (generated along with depth and normals). We find that our generated depth is comparable to depth predicted by [25] while normals from our model are significantly better.

C.3. Monocular depth and normal estimation

Internet images: We show more depth and normal predictions on in-the-wild images produced by Orchid in Figures 14, 15, 16, and 17. Figures 14 and 15 compare our joint predictions to those from GeoWizard [13]. We find that our depth and normals are more accurate (with fewer errors on large sections), even though GeoWizard’s predictions more detailed in many cases. In Figures 16, and 17, we compare Orchid’s predictions to Marigold [25]. We find that Orchid has better depth estimates at longer ranges, and significantly

better normal estimates overall. Note that we need different Marigold weights to predict depth and normals (unlike our joint prediction model). When comparing colorized depth maps on these datasets without ground truth depth, please refer to the note in Section C.1.

Zero-shot benchmark images: We show more depth and normal predictions on the zero-shot depth and normal estimation benchmarks using in Section 4 of our paper in Figures 19, 18, and 20. Figure 19 shows that Orchid is competitive with diffusion-based depth prediction baselines Marigold [25] and GeoWizard [13], while being slightly better in some cases. Both [25] and [13] have a common failure mode where depth estimates are sensitive to image discontinuities, which our model is significantly less sensitive to. Figure 18 shows that our model is significantly better at depth estimation in outdoor environments, especially at longer ranges. Figure 20 shows that our model is significantly better at surface normals estimation, particularly on objects with curved surfaces.

C.4. Joint inpainting

Section 4.4 explains how our model can be used to jointly inpaint color-depth-normals. For this task, we use as input paired color, depth, and normal images, and a user-provided mask for the region to be inpainted. In cases where only a color image is available, depth and normals can be generated using the image-conditioned Orchid. We then generate the latents in the masked region, using Orchid to iteratively denoise them, while using noise-free latents encoded from the inputs for the unmasked region. This is similar to the approach proposed in RePaint [35]. We provide qualitative results in Figure 21. We show multiple inpainting results for the same input. We find that Orchid is able to jointly generate different semantically and geometrically consistent color, depth, and normals for the masked regions.

C.5. 3D reconstruction from single view

The image-conditioned Orchid can jointly generate depth and normals from an input image. These color, depth, and surface normals can be used to reconstruct the 3D scene using either Gaussian Splatting methods (3DGS [26], 2DGS [23]) or Poisson surface reconstruction. We provide results at: <https://orchid3d.github.io>.

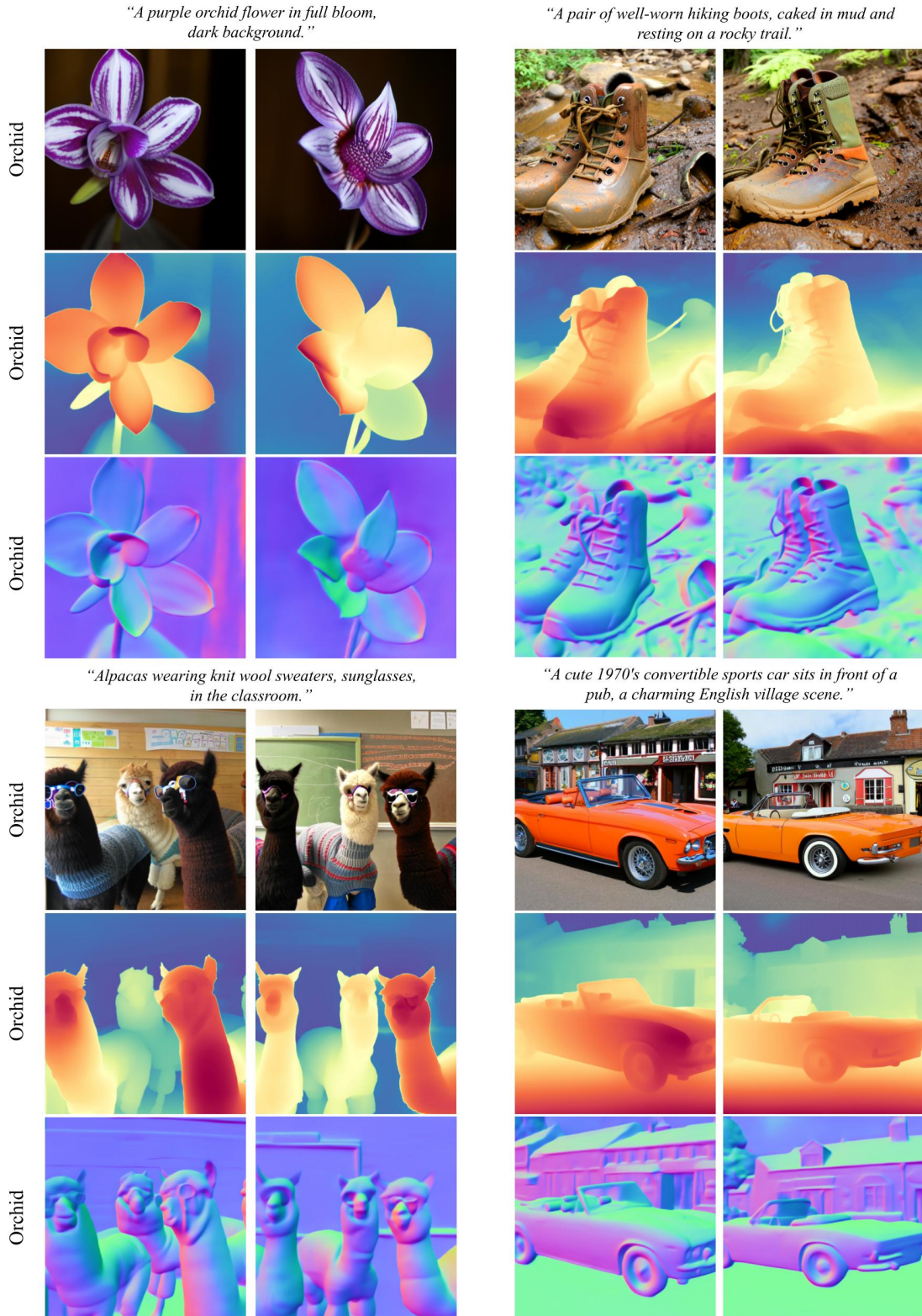
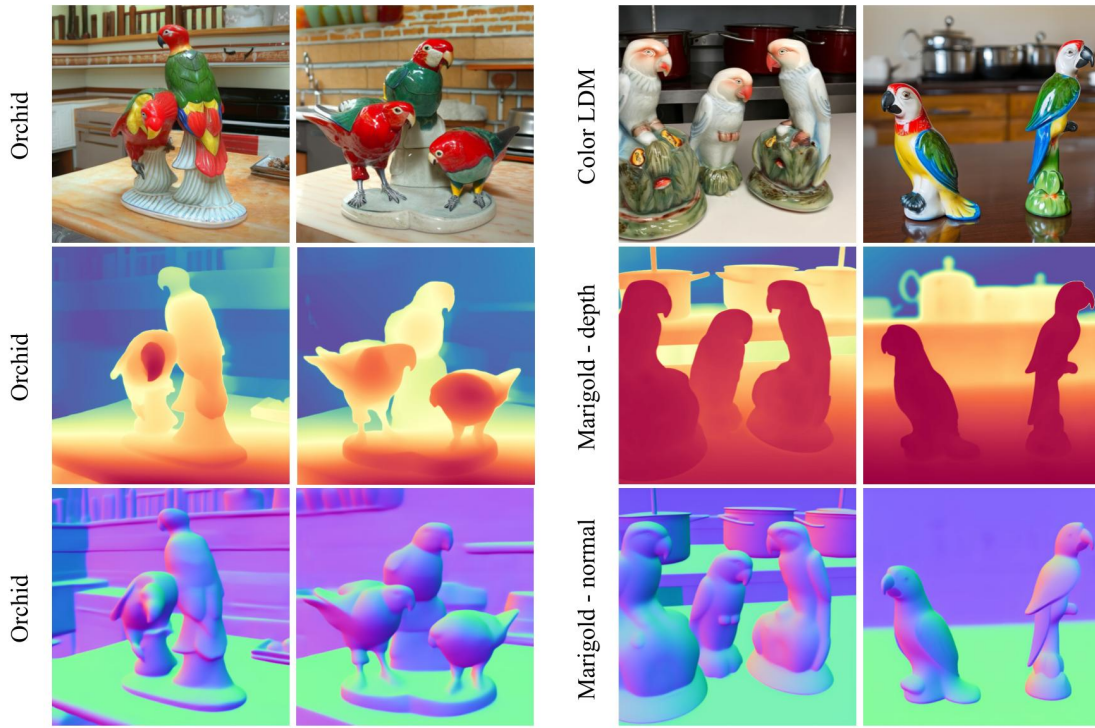


Figure 11. **Text conditioned generation:** We show color, depth and normals generated by Orchid for different text prompts. We show two results for each prompt.

"Porcelain statues of parrots in the kitchen, with cooking pots in the background"



"A husky dressed up as Santa Claus on a boat."

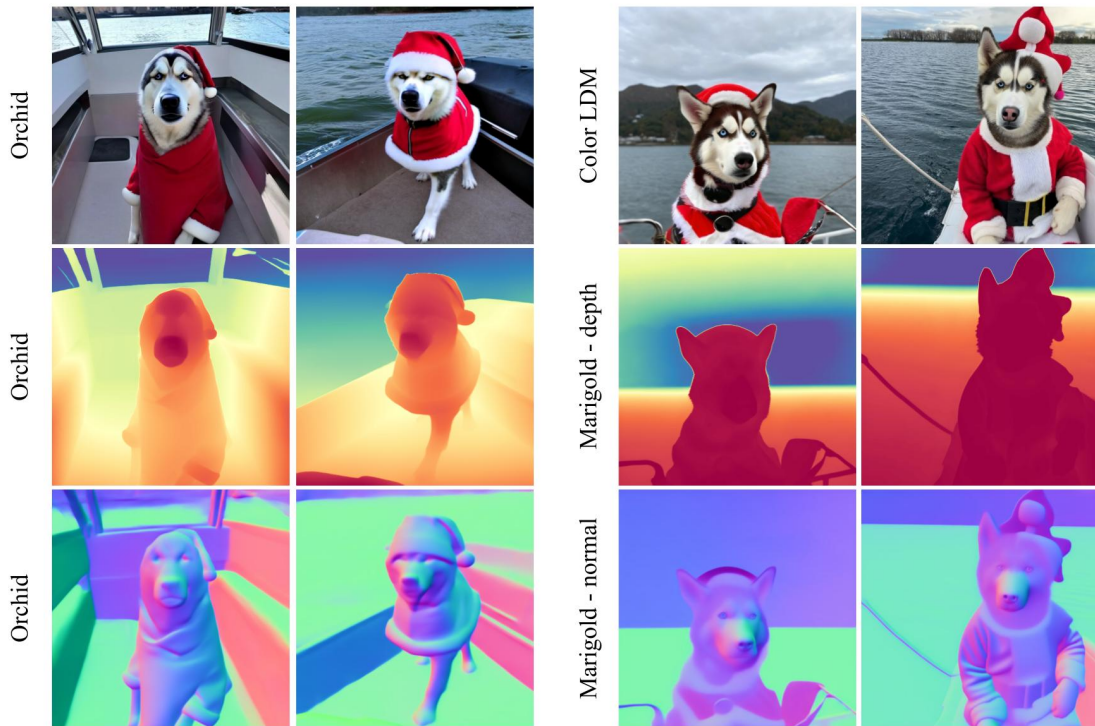
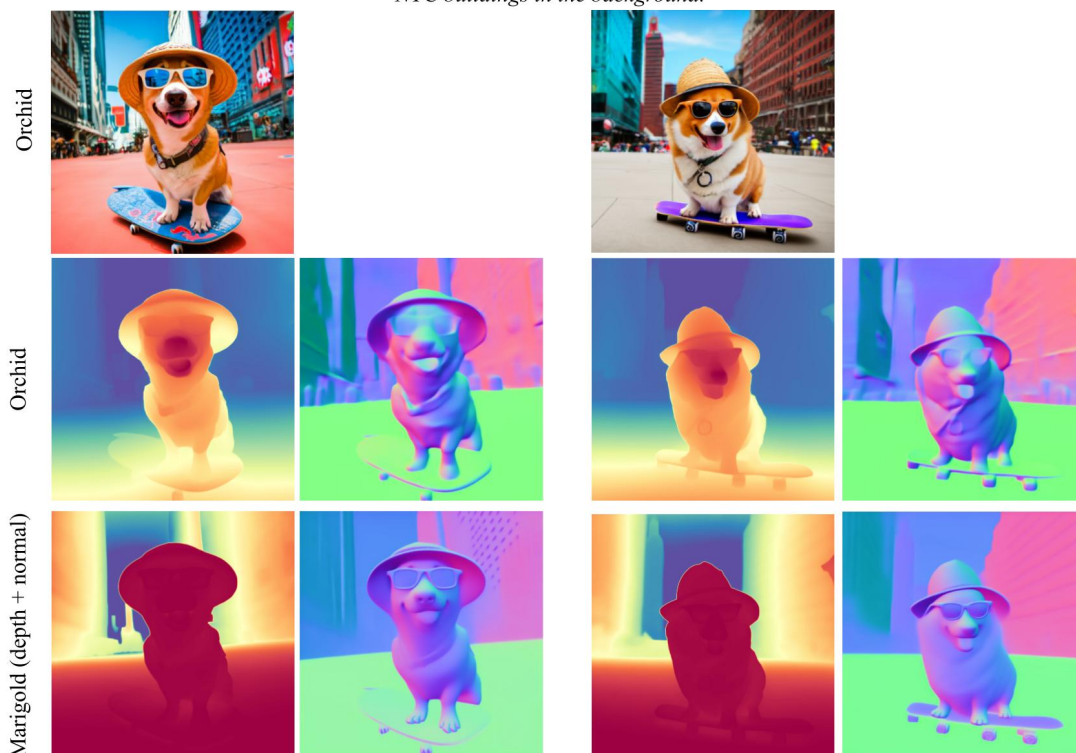


Figure 12. **Text conditioned color-depth-normal generation:** We show two predictions from Orchid for each text prompt. We qualitatively compare these to the alternative: generate color, depth and normals from a separate diffusion model for each. For this baseline, we use a color-only LDM for color, and separate Marigold [25] models for depth and normals. When comparing results, please refer to our note on depth map visualization (Section C.1).

“A Corgi dog on a skateboard in Times Square. It is wearing sunglasses and a beach hat. NYC buildings in the background.”



“A bedroom with a pretty canopy bed, fluffy pillows and a dresser with a mirror”

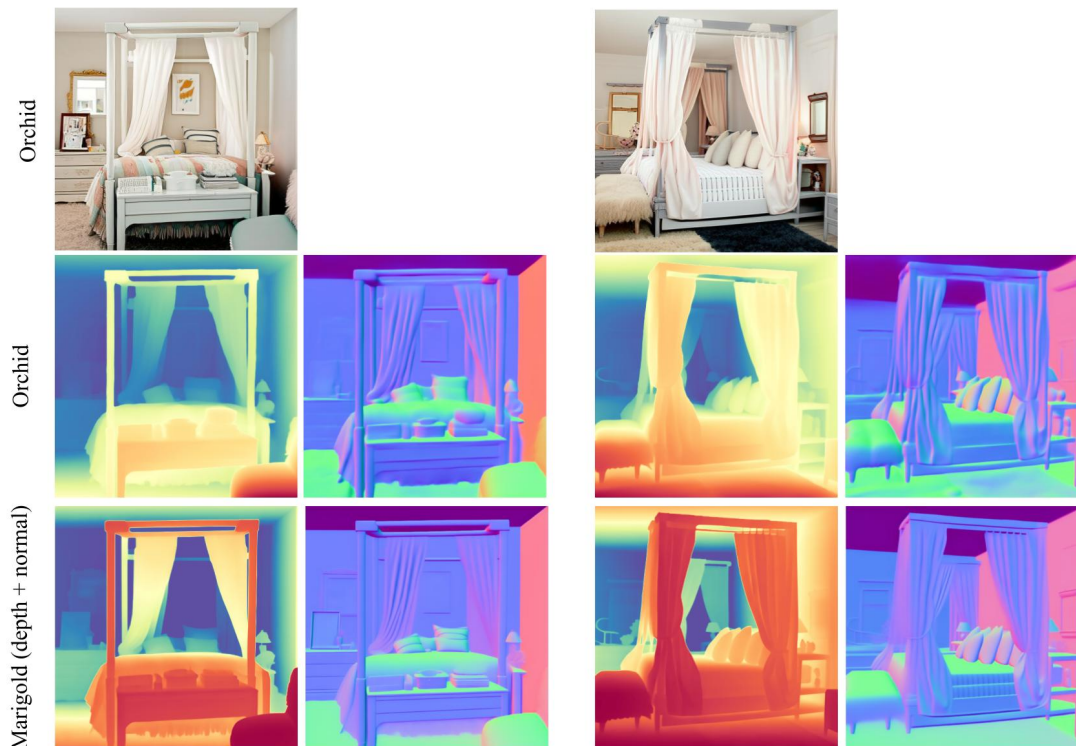


Figure 13. **Text conditioned color-depth-normal generation:** We show two predictions from Orchid for each text prompt. We compare the geometry predicted by our model to Marigold [25] which uses separate models for depth and normal. When comparing results, please refer to our note on depth map visualization (Section C.1).

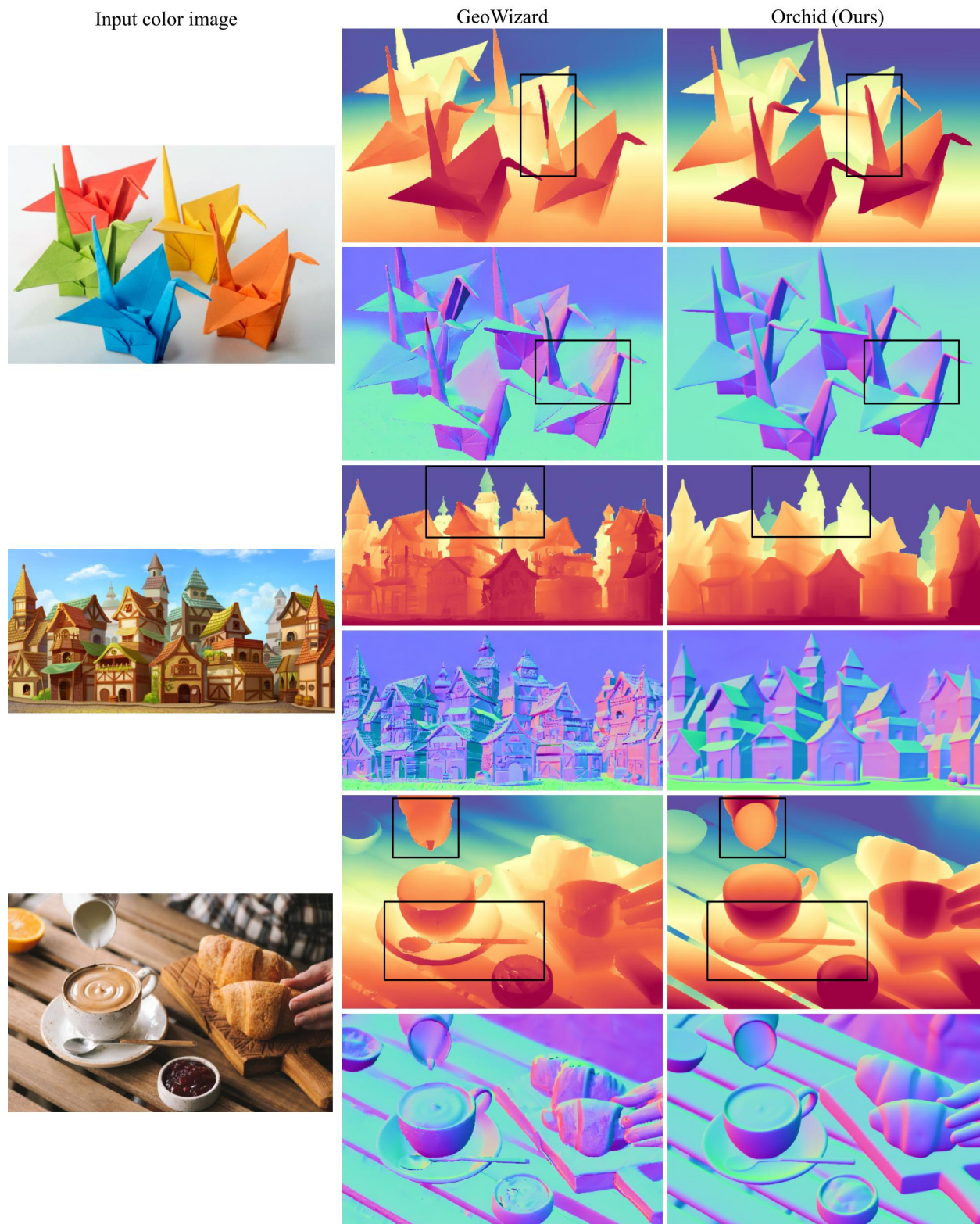


Figure 14. Comparison of GeoWizard [13] and Orchid for depth and normal estimation on in-the-wild input images. We can see that unlike GeoWizard, results from Orchid have correct depth and normal predictions while still having sharp boundaries. Some of these areas have been highlighted in the images shown above. In particular, Orchid shows less discontinuities in the Origami surfaces in both depth and normals, and more accurate depth predictions of the hollow objects pictured (milk pitcher, coffee mug and saucer).

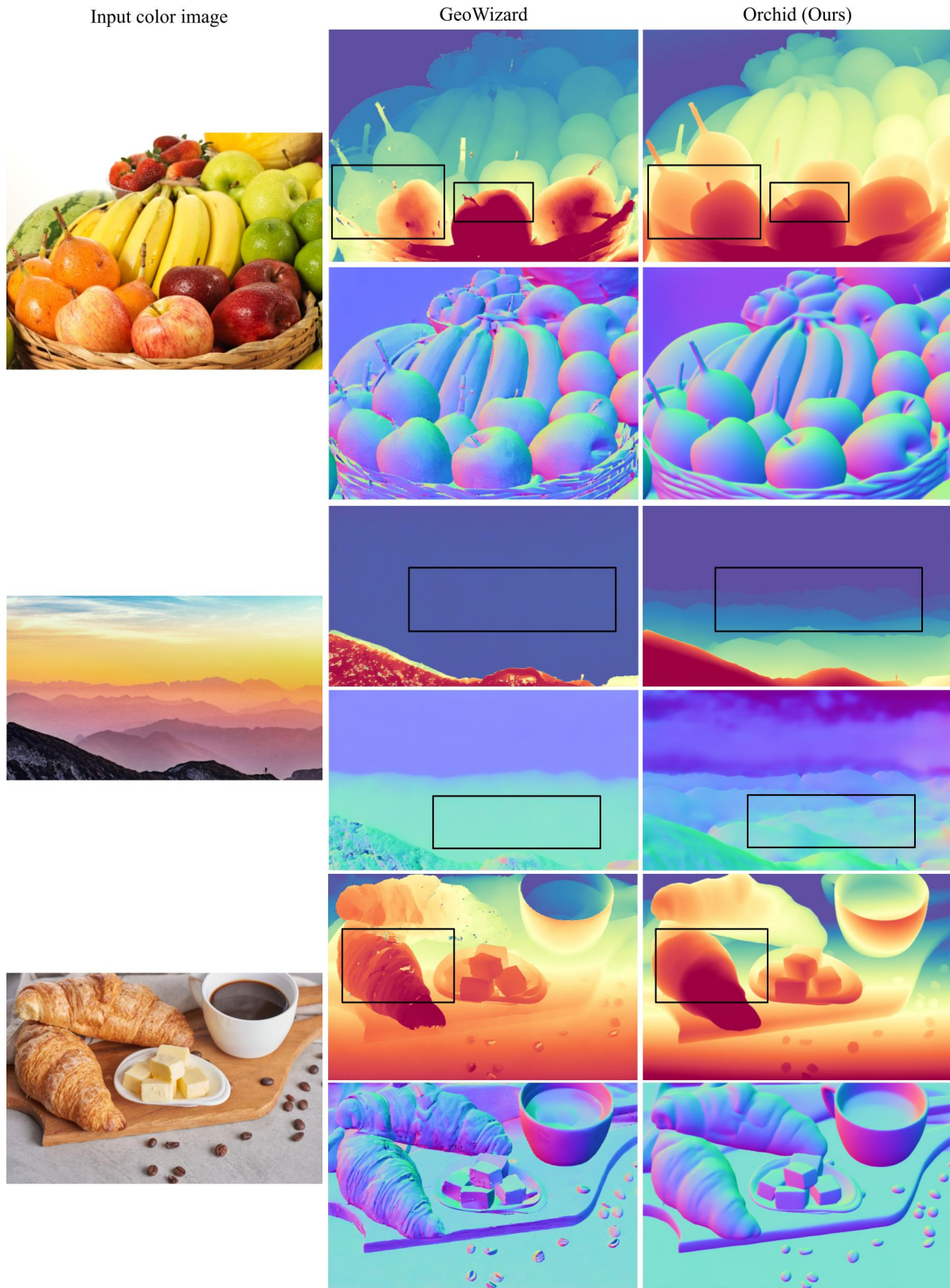


Figure 15. Comparison of GeoWizard [13] and Orchid on in-the-wild input images. Some areas with larger differences have been highlighted. In particular, we observe that high-frequency parts of the image can manifest themselves in noisy depth and normal predictions by GeoWizard (highlights on the fruits, texture of the croissants), whereas Orchid correctly predicts smooth surfaces. In far-away layered scenes we also observe that GeoWizard’s predictions do not cover background (mountain range example).

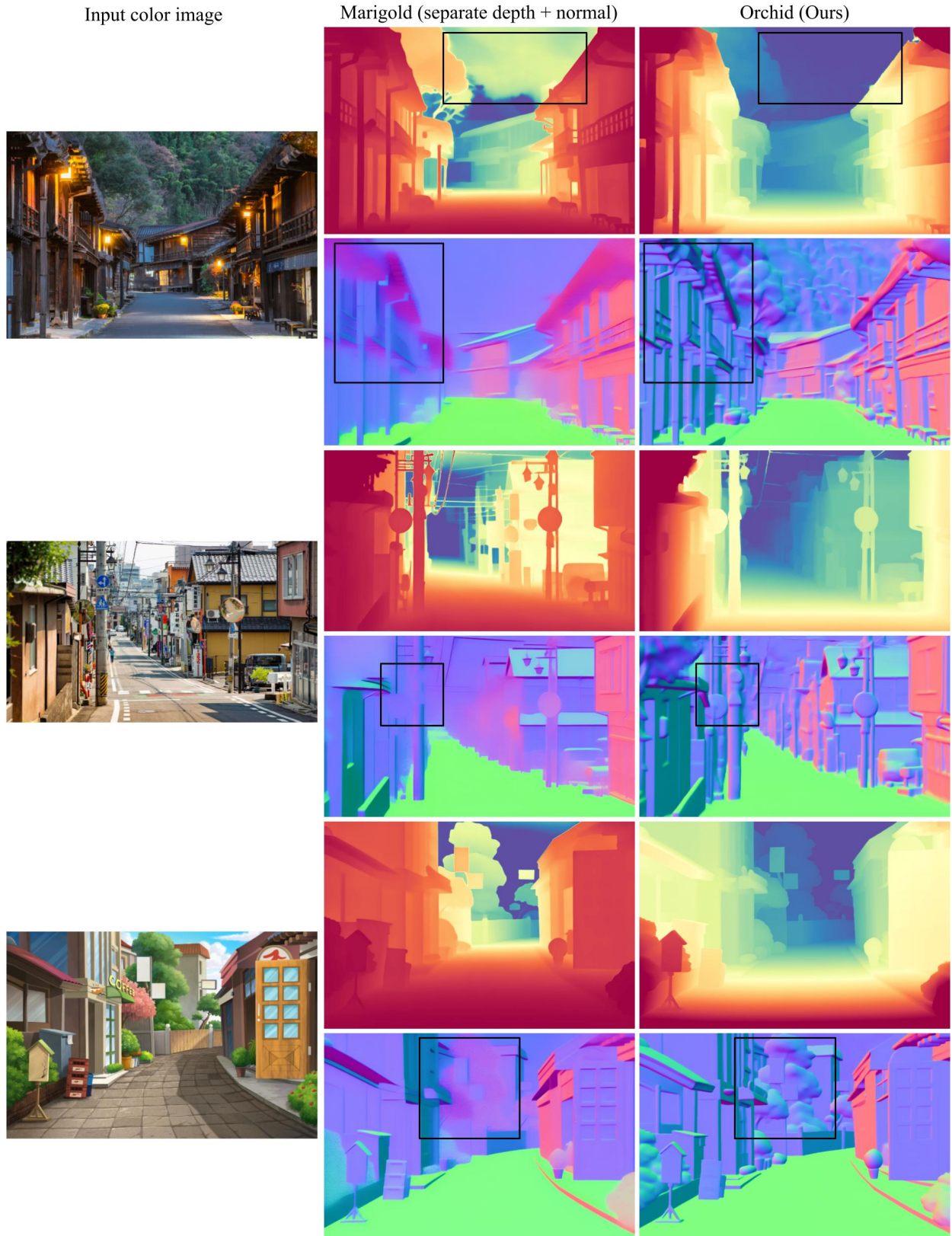


Figure 16. Comparison of Marigold [25] and Orchid on some in-the-wild input images. We use separate Marigold models to predict depth and normals. Orchid’s joint predictions are better, especially for surface normals. Some notable differences are highlighted above.

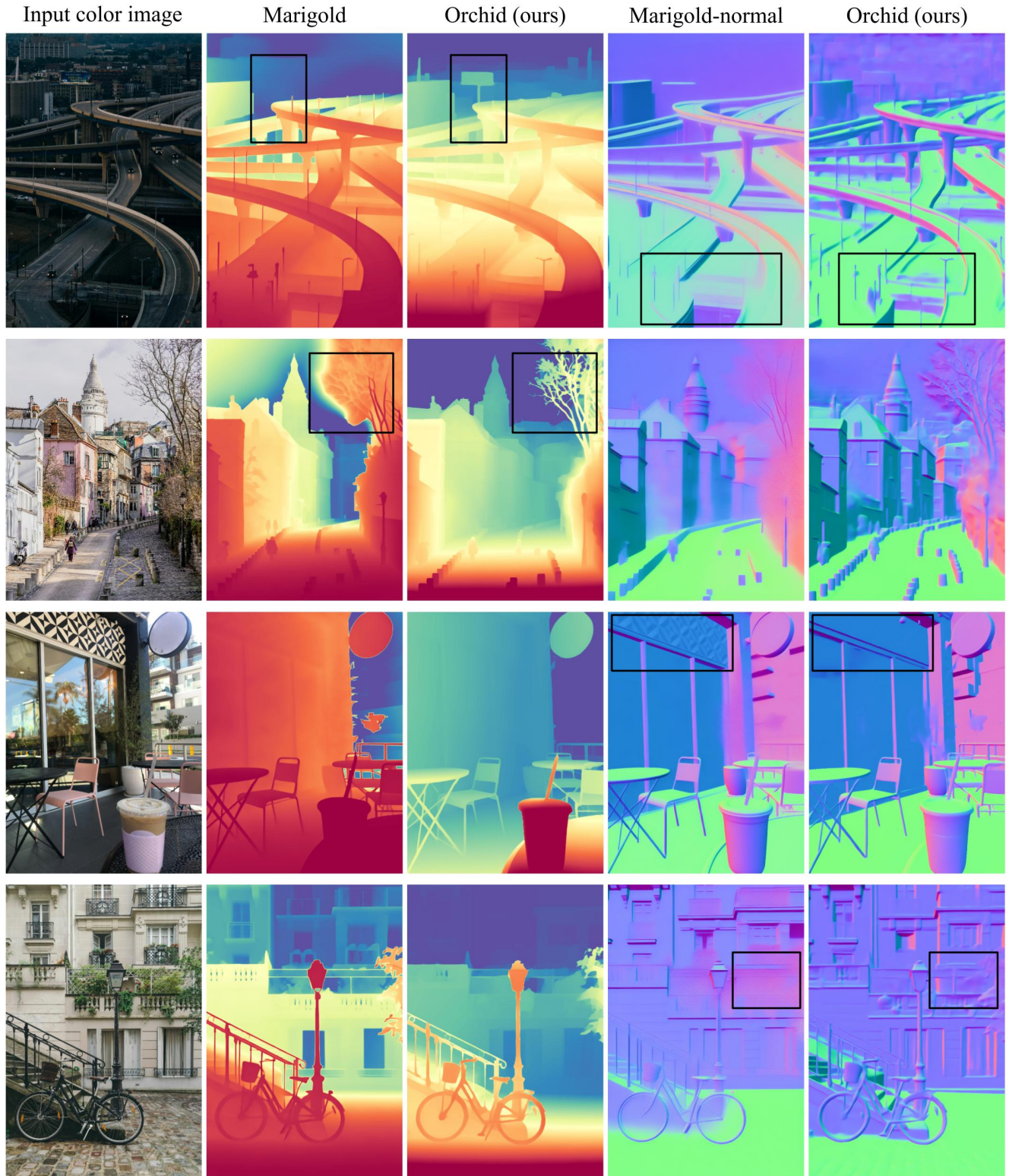


Figure 17. Comparison of Marigold [25] and Orchid on some in-the-wild input images. We can clearly see that our model Orchid can correctly predicts depth and surface normal of both far-away and nearby objects. Depth-maps from Orchid also has sharper and more accurate boundaries near pixels with depth discontinuities (*e.g.* between narrow tree branches and sky). Some of these are highlighted in the figure above.

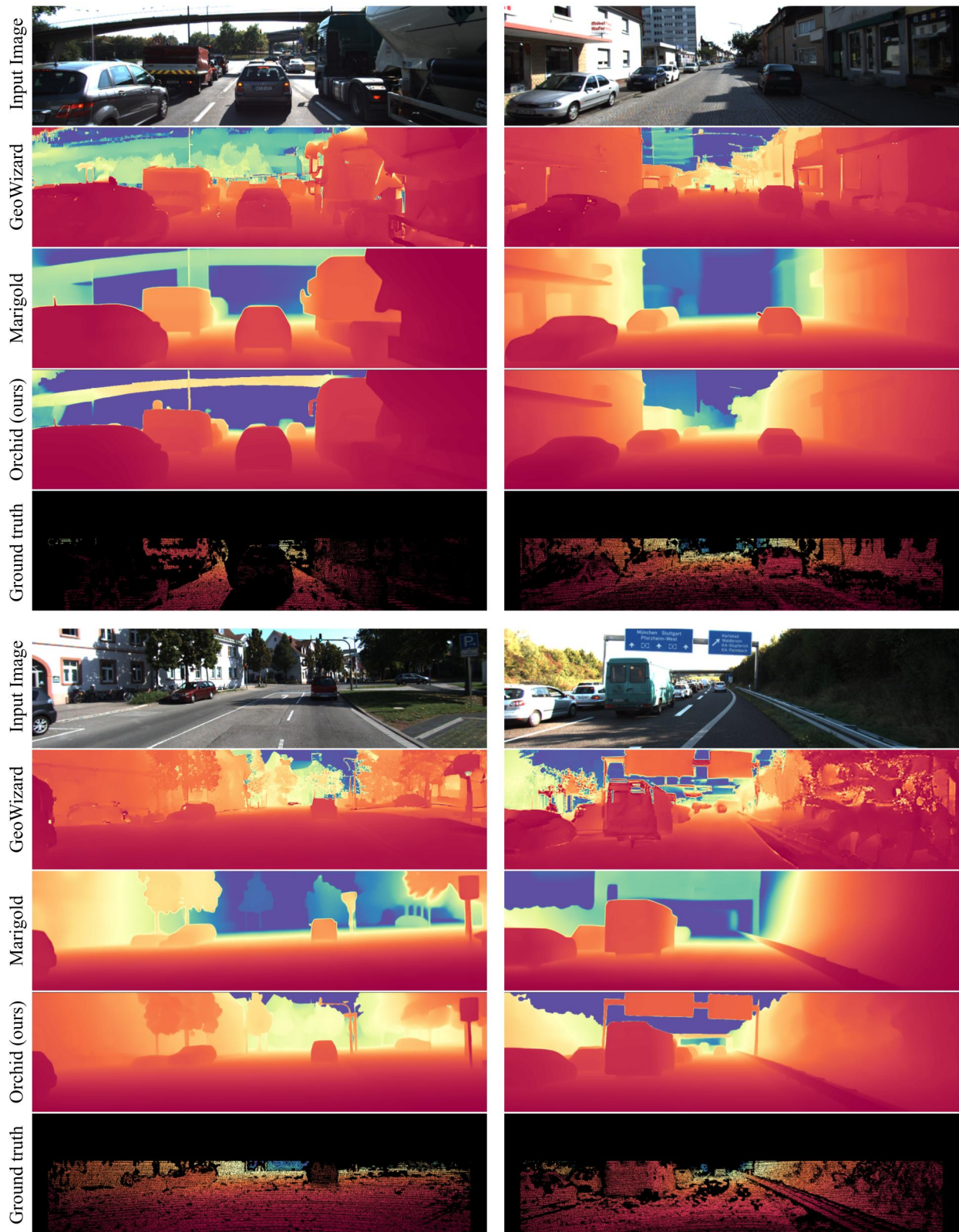


Figure 18. Qualitative comparison of monocular depth prediction on KITTI [15] dataset between GeoWizard [13], Marigold [25] and Orchid. Ground-truth depth (from lidar) are shown in the bottom row. Pixels without valid ground-truth depth are colored black. Orchid’s predictions are significantly better, especially at longer ranges.

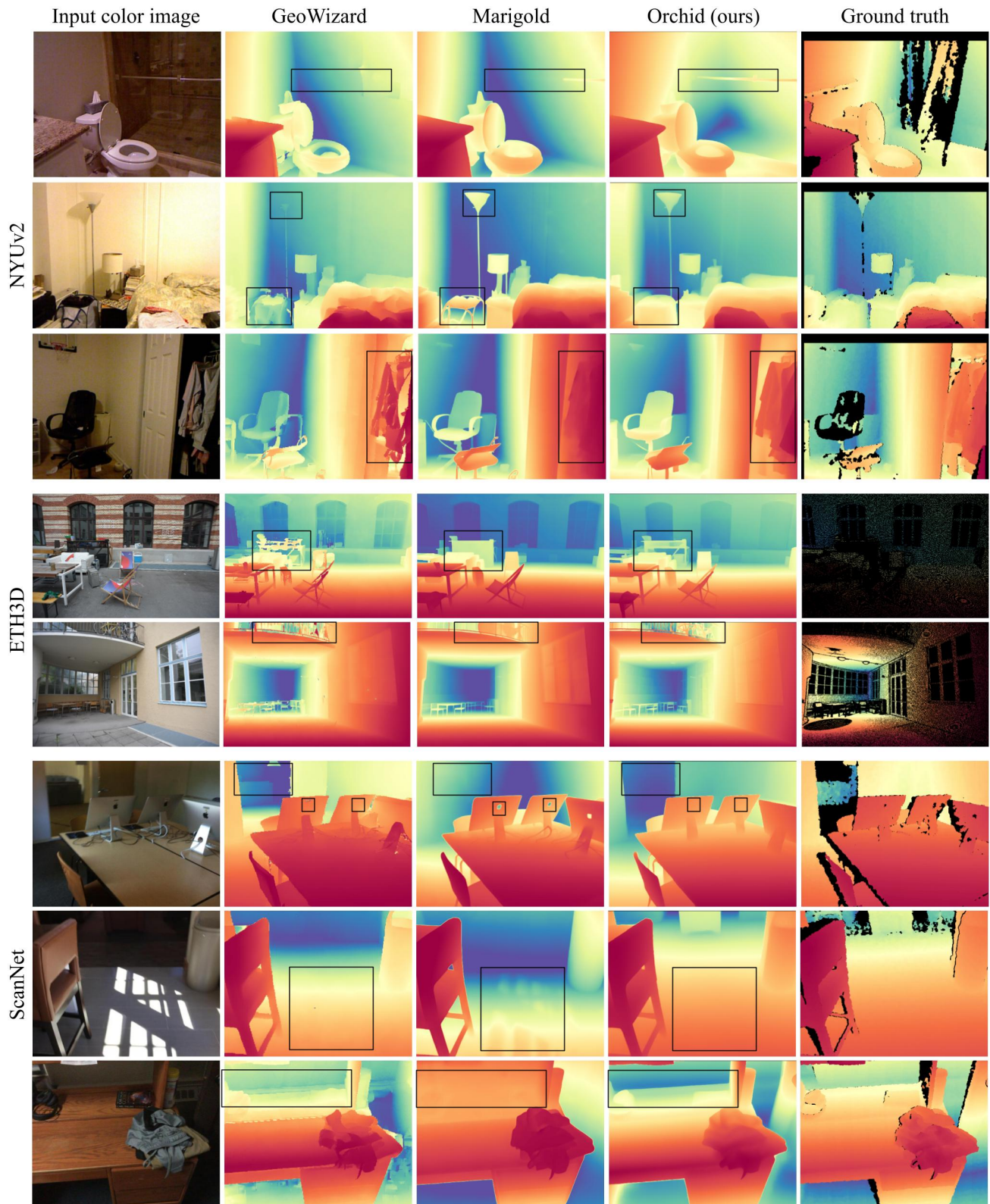


Figure 19. Comparison of monocular depth prediction results by GeoWizard [13], Marigold [25] and Orchid on NYUv2 [36], ETH3D [50], and ScanNet [7] datasets. Ground-truth depth are shown in the rightmost column. Pixels without valid ground-truth depth are colored black. Our model Orchid has better depth predictions. Some notable differences are highlighted.

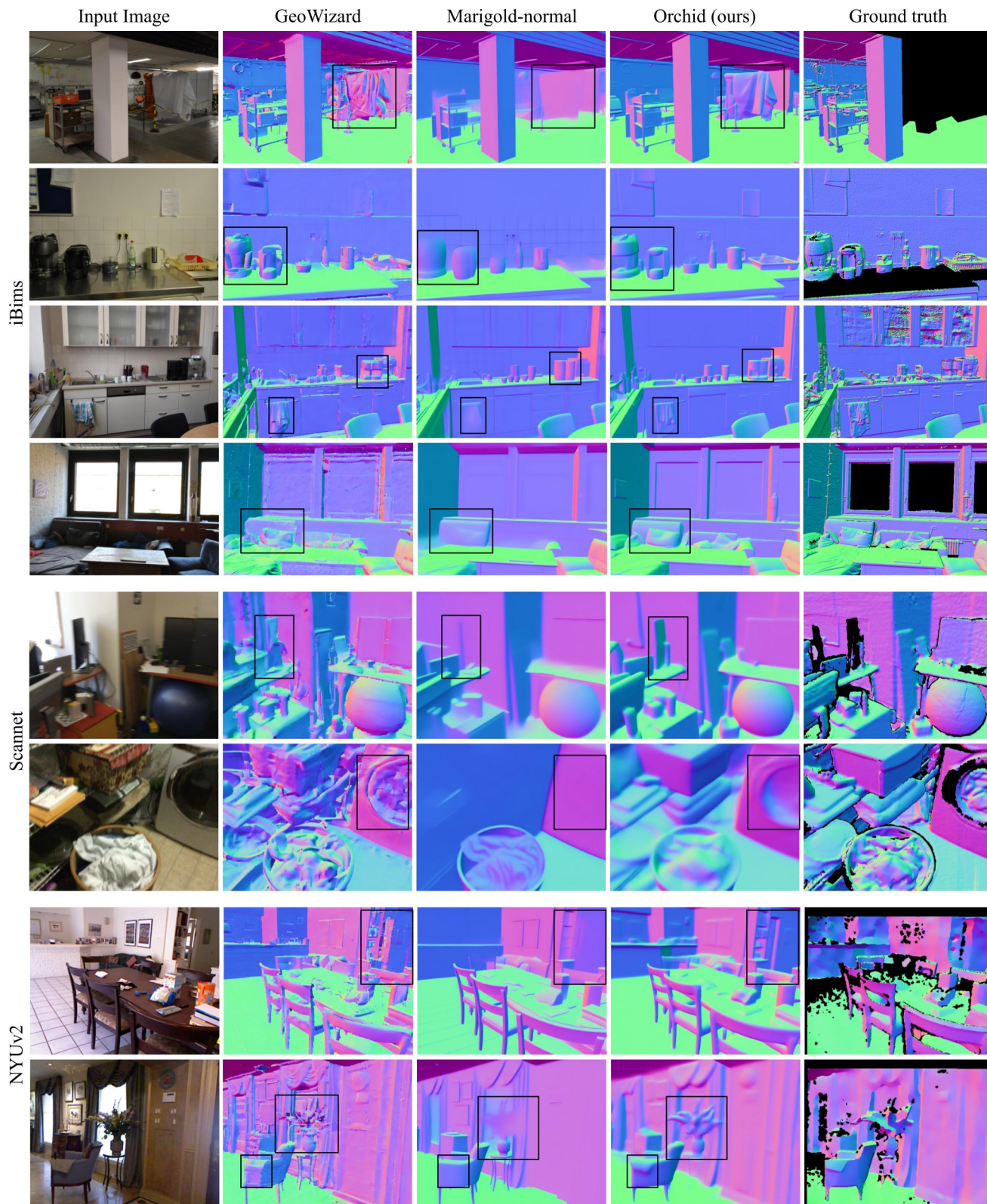


Figure 20. We compare single color image to surface-normal prediction methods of GeoWizard [13], Marigold [25] and Orchid on iBims [28], and ScanNet [7], and NYUv2 [36] datasets. Ground-truth normal are shown in the rightmost column. Pixels without valid ground-truth normal are colored black. Some notable differences are highlighted. Orchid’s normals are significantly better than baselines.

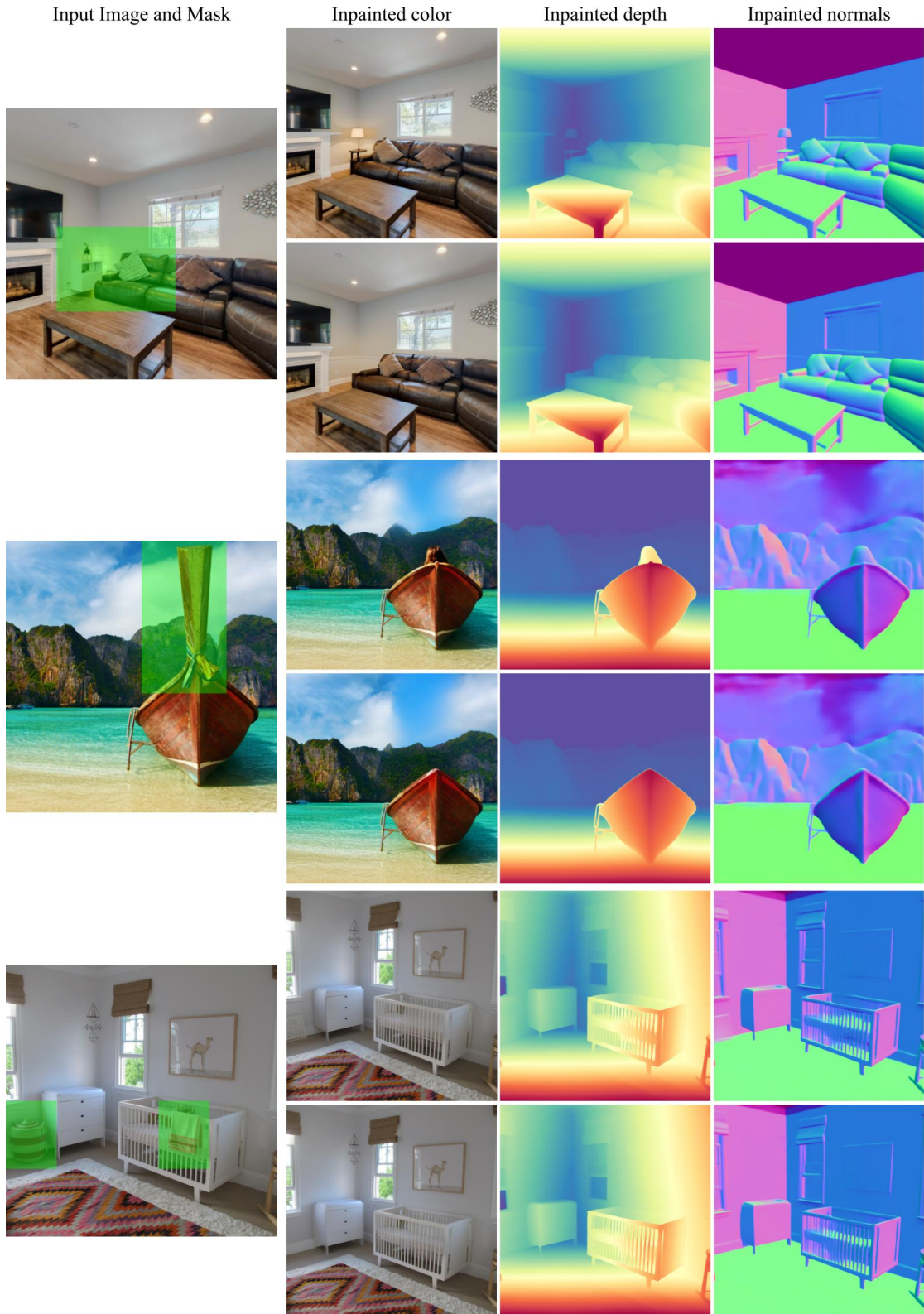


Figure 21. **Joint color-depth-normal inpainting:** Given color-depth-normal images with masked regions, our model inpaints them jointly. Masked-out pixels are shown with green overlays on the input images in the leftmost column. As demonstrated in the results above, inpainted outputs from Orchid look very realistic. For *e.g.* in top row, the inpainted pillow seems to also have a similar color theme as the other pillow and the sofa. The inpainted results are also diverse (*e.g.* the canoe with and without the girl in the second example).

References

- [1] Hassan Abu Alhajja, Siva Karthik Mustikovela, Lars Mescheder, Andreas Geiger, and Carsten Rother. Augmented reality meets computer vision: Efficient data generation for urban driving scenes. *International Journal of Computer Vision*, 126(9):961–972, 2018. 1
- [2] Gwangbin Bae and Andrew J. Davison. Rethinking inductive biases for surface normal estimation. In *CVPR*, 2024. 2, 7
- [3] Shariq Farooq Bhat, Ibraheem Alhashim, and Peter Wonka. Adabins: Depth estimation using adaptive bins. In *CVPR*, pages 4009–4018, 2021. 2
- [4] Daniel J Butler, Jonas Wulff, Garrett B Stanley, and Michael J Black. A naturalistic open source movie for optical flow evaluation. In *ECCV*, pages 611–625. Springer, 2012. 7
- [5] Yun Chen, Frieda Rong, Shivam Duggal, Shenlong Wang, Xinchun Yan, Sivabalan Manivasagam, Shangjie Xue, Ersin Yumer, and Raquel Urtasun. Geosim: Realistic video simulation via geometry-aware composition for self-driving. In *CVPR*, 2021. 1
- [6] Hyungjin Chung, Jeongsol Kim, Michael Thompson McCann, Marc Louis Klasky, and Jong Chul Ye. Diffusion posterior sampling for general noisy inverse problems. In *The Eleventh International Conference on Learning Representations*, 2023. 3
- [7] Angela Dai, Angel X. Chang, Manolis Savva, Maciej Halber, Thomas Funkhouser, and Matthias Nießner. Scannet: Richly-annotated 3d reconstructions of indoor scenes. In *CVPR*, 2017. 6, 7, 19, 20
- [8] Yiqun Duan, Xianda Guo, and Zheng Zhu. Diffusiondepth: Diffusion denoising approach for monocular depth estimation. In *ECCV*, 2024. 3
- [9] Ainaz Eftekhari, Alexander Sax, Jitendra Malik, and Amir Zamir. Omnidata: A scalable pipeline for making multi-task mid-level vision datasets from 3d scans. In *ICCV*, pages 10786–10796, 2021. 2, 5, 7
- [10] David Eigen and Rob Fergus. Predicting depth, surface normals and semantic labels with a common multi-scale convolutional architecture. In *ICCV*, pages 2650–2658, 2015. 3
- [11] David Eigen, Christian Puhusch, and Rob Fergus. Depth map prediction from a single image using a multi-scale deep network. *NIPS*, 27, 2014. 2
- [12] Huan Fu, Mingming Gong, Chaohui Wang, Kayhan Batmanghelich, and Dacheng Tao. Deep ordinal regression network for monocular depth estimation. In *CVPR*, pages 2002–2011, 2018.
- [13] Xiao Fu, Wei Yin, Mu Hu, Kaixuan Wang, Yuexin Ma, Ping Tan, Shaojie Shen, Dahua Lin, and Xiaoxiao Long. Geowizard: Unleashing the diffusion priors for 3d geometry estimation from a single image. In *ECCV*, 2024. 2, 3, 4, 6, 7, 10, 14, 15, 18, 19, 20
- [14] Adrien Gaidon, Qiao Wang, Yohann Cabon, and Eleonora Vig. Virtual worlds as proxy for multi-object tracking analysis. In *CVPR*, pages 4340–4349, 2016. 1, 5
- [15] Andreas Geiger, Philip Lenz, and Raquel Urtasun. Are we ready for autonomous driving? the kitti vision benchmark suite. In *CVPR*, 2012. 6, 18
- [16] Vitor Guizilini, Igor Vasiljevic, Dian Chen, Rareş Ambruş, and Adrien Gaidon. Towards zero-shot scale-aware monocular depth estimation. In *ICCV*, pages 9233–9243, 2023. 2
- [17] Abhinav Gupta, Alexei A Efros, and Martial Hebert. Blocks world revisited: Image understanding using qualitative geometry and mechanics. In *ECCV*. Springer, 2010. 1
- [18] Jing He, Haodong Li, Wei Yin, Yixun Liang, Leheng Li, Kaiqiang Zhou, Hongbo Liu, Bingbing Liu, and Ying-Cong Chen. Lotus: Diffusion-based visual foundation model for high-quality dense prediction. *arXiv preprint arXiv:2409.18124*, 2024. 2, 4, 7
- [19] Jonathan Ho and Tim Salimans. Classifier-free diffusion guidance, 2022. 4
- [20] Jonathan Ho, Ajay Jain, and Pieter Abbeel. Denoising diffusion probabilistic models. In *NeurIPS*, 2020. 4, 5
- [21] Derek Hoiem, Alexei A. Efros, and Martial Hebert. Automatic photo pop-up. *ACM Trans. Graph.*, 24(3):577–584, 2005. 1
- [22] Mu Hu, Wei Yin, Chi Zhang, Zhipeng Cai, Xiaoxiao Long, Hao Chen, Kaixuan Wang, Gang Yu, Chunhua Shen, and Shaojie Shen. Metric3d v2: A versatile monocular geometric foundation model for zero-shot metric depth and surface normal estimation. *arXiv preprint arXiv:2404.15506*, 2024. 2, 3, 5, 6, 9
- [23] Binbin Huang, Zehao Yu, Anpei Chen, Andreas Geiger, and Shenghua Gao. 2d gaussian splatting for geometrically accurate radiance fields. In *SIGGRAPH 2024 Conference Papers*. Association for Computing Machinery, 2024. 10
- [24] Yuanfeng Ji, Zhe Chen, Enze Xie, Lanqing Hong, Xihui Liu, Zhaoqiang Liu, Tong Lu, Zhenguo Li, and Ping Luo. Ddp: Diffusion model for dense visual prediction. In *ICCV*, pages 21741–21752, 2023. 3
- [25] Bingxin Ke, Anton Obukhov, Shengyu Huang, Nando Metzger, Rodrigo Caye Daudt, and Konrad Schindler. Repurposing diffusion-based image generators for monocular depth estimation. In *CVPR*, 2024. 2, 3, 4, 6, 7, 8, 10, 12, 13, 16, 17, 18, 19, 20
- [26] Bernhard Kerbl, Georgios Kopanas, Thomas Leimkühler, and George Drettakis. 3d gaussian splatting for real-time radiance field rendering. *ACM Transactions on Graphics*, 42(4), 2023. 1, 6, 10
- [27] Diederik P Kingma. Auto-encoding variational bayes. *arXiv preprint arXiv:1312.6114*, 2013. 4
- [28] Tobias Koch, Lukas Liebel, Friedrich Fraundorfer, and Marco Korner. Evaluation of cnn-based single-image depth estimation methods. In *ECCV Workshops*, pages 0–0, 2018. 7, 20
- [29] Bo Li, Chunhua Shen, Yuchao Dai, Anton Van Den Hengel, and Mingyi He. Depth and surface normal estimation from monocular images using regression on deep features and hierarchical crfs. In *CVPR*, pages 1119–1127, 2015. 3
- [30] Zhengqi Li and Noah Snavely. Megadepth: Learning single-view depth prediction from internet photos. In *CVPR*, pages 2041–2050, 2018. 2, 4
- [31] Jie Liang, Hui Zeng, and Lei Zhang. Details or artifacts: A locally discriminative learning approach to realistic image super-resolution. In *CVPR*, 2022. 4

- [32] Chen-Hsuan Lin, Jun Gao, Luming Tang, Towaki Takikawa, Xiao-hui Zeng, Xun Huang, Karsten Kreis, Sanja Fidler, Ming-Yu Liu, and Tsung-Yi Lin. Magic3d: High-resolution text-to-3d content creation. In *CVPR*, pages 300–309, 2023. 3
- [33] Shanchuan Lin, Bingchen Liu, Jiashi Li, and Xiao Yang. Common diffusion noise schedules and sample steps are flawed, 2024. 5
- [34] Ruoshi Liu, Rundi Wu, Basile Van Hoorick, Pavel Tokmakov, Sergey Zakharov, and Carl Vondrick. Zero-1-to-3: Zero-shot one image to 3d object. In *ICCV*, pages 9298–9309, 2023. 3
- [35] Andreas Lugmayr, Martin Danelljan, Andres Romero, Fisher Yu, Radu Timofte, and Luc Van Gool. Repaint: Inpainting using denoising diffusion probabilistic models. In *CVPR*, 2022. 3, 8, 10
- [36] Pushmeet Kohli, Nathan Silberman, Derek Hoiem, and Rob Fergus. Indoor segmentation and support inference from rgbd images. In *ECCV*, 2012. 6, 7, 19, 20
- [37] Maxime Oquab, Timothée Darcet, Theo Moutakanni, Huy V. Vo, Marc Szafranec, Vasil Khalidov, Pierre Fernandez, Daniel Haziza, Francisco Massa, Alaaeldin El-Nouby, Russell Howes, Po-Yao Huang, Hu Xu, Vasu Sharma, Shang-Wen Li, Wojciech Galuba, Mike Rabbat, Mido Assran, Nicolas Ballas, Gabriel Synnaeve, Ishan Misra, Herve Jegou, Julien Mairal, Patrick Labatut, Armand Joulin, and Piotr Bojanowski. DINOv2: Learning robust visual features without supervision, 2023. 3
- [38] Ben Poole, Ajay Jain, Jonathan T. Barron, and Ben Mildenhall. Dreamfusion: Text-to-3d using 2d diffusion. In *ICLR*, 2023. 3
- [39] René Ranftl, Katrin Lasinger, David Hafner, Konrad Schindler, and Vladlen Koltun. Towards robust monocular depth estimation: Mixing datasets for zero-shot cross-dataset transfer. *IEEE Transactions on Pattern Analysis and Machine Intelligence*, 44(3):1623–1637, 2022. 2, 6, 7
- [40] Mike Roberts, Jason Ramapuram, Anurag Ranjan, Atulit Kumar, Miguel Angel Bautista, Nathan Paczan, Russ Webb, and Joshua M. Susskind. Hypersim: A photorealistic synthetic dataset for holistic indoor scene understanding. In *ICCV*, 2021. 5
- [41] Robin Rombach, Andreas Blattmann, Dominik Lorenz, Patrick Esser, and Björn Ommer. High-resolution image synthesis with latent diffusion models. In *Proceedings of the IEEE/CVF conference on computer vision and pattern recognition*, pages 10684–10695, 2022. 4, 5
- [42] Litu Rout, Negin Raof, Giannis Daras, Constantine Caramanis, Alex Dimakis, and Sanjay Shakkottai. Solving linear inverse problems provably via posterior sampling with latent diffusion models. In *Thirty-seventh Conference on Neural Information Processing Systems*, 2023. 3
- [43] L Rout, Y Chen, A Kumar, C Caramanis, S Shakkottai, and W Chu. Beyond first-order tweedie: Solving inverse problems using latent diffusion, 2024. 3
- [44] Shunsuke Saito, Zeng Huang, Ryota Natsume, Shigeo Morishima, Angjoo Kanazawa, and Hao Li. Pifu: Pixel-aligned implicit function for high-resolution clothed human digitization. In *ICCV*, pages 2304–2314, 2019. 1
- [45] Tim Salimans and Jonathan Ho. Progressive distillation for fast sampling of diffusion models. In *ICLR*, 2022. 4
- [46] Manolis Savva, Abhishek Kadian, Oleksandr Maksymets, Yili Zhao, Erik Wijmans, Bhavana Jain, Julian Straub, Jia Liu, Vladlen Koltun, Jitendra Malik, et al. Habitat: A platform for embodied ai research. In *ICCV*, pages 9339–9347, 2019. 1
- [47] Ashutosh Saxena, Min Sun, and Andrew Y Ng. Make3d: Learning 3d scene structure from a single still image. *IEEE transactions on pattern analysis and machine intelligence*, 31(5):824–840, 2008. 1
- [48] Saurabh Saxena, Abhishek Kar, Mohammad Norouzi, and David J Fleet. Monocular depth estimation using diffusion models. *arXiv preprint arXiv:2302.14816*, 2023. 3
- [49] Saurabh Saxena, Charles Herrmann, Junhwa Hur, Abhishek Kar, Mohammad Norouzi, Deqing Sun, and David J Fleet. The surprising effectiveness of diffusion models for optical flow and monocular depth estimation. *NeurIPS*, 36, 2024. 3
- [50] Thomas Schops, Johannes L Schonberger, Silvano Galliani, Torsten Sattler, Konrad Schindler, Marc Pollefeys, and Andreas Geiger. A multi-view stereo benchmark with high-resolution images and multi-camera videos. In *CVPR*, pages 3260–3269, 2017. 6, 19
- [51] Julian Straub, Thomas Whelan, Lingni Ma, Yufan Chen, Erik Wijmans, Simon Green, Jakob J Engel, Raul Mur-Artal, Carl Ren, Shobhit Verma, et al. The replica dataset: A digital replica of indoor spaces. *arXiv preprint arXiv:1906.05797*, 2019. 1
- [52] Marshall Tappen, William Freeman, and Edward Adelson. Recovering intrinsic images from a single image. *NIPS*, 15, 2002. 1
- [53] Igor Vasiljevic, Nick Kolkin, Shanyi Zhang, Ruotian Luo, Haochen Wang, Falcon Z. Dai, Andrea F. Daniele, Mohammadreza Mostajabi, Steven Basart, Matthew R. Walter, and Gregory Shakhnarovich. DIODE: A Dense Indoor and Outdoor DDepth Dataset. *CoRR*, abs/1908.00463, 2019. 5
- [54] Xiaolong Wang, David Fouhey, and Abhinav Gupta. Designing deep networks for surface normal estimation. In *CVPR*, pages 539–547, 2015. 2
- [55] Zhengyi Wang, Cheng Lu, Yikai Wang, Fan Bao, Chongxuan Li, Hang Su, and Jun Zhu. Prolificdreamer: High-fidelity and diverse text-to-3d generation with variational score distillation. *NeurIPS*, 36, 2024. 3
- [56] Daniel Winter, Matan Cohen, Shlomi Fruchter, Yael Pritch, Alex Rav-Acha, and Yedid Hoshen. Objectdrop: Bootstrapping counterfactuals for photorealistic object removal and insertion, 2024. 3
- [57] Dan Xu, Wanli Ouyang, Xiaogang Wang, and Nicu Sebe. Pad-net: Multi-tasks guided prediction-and-distillation network for simultaneous depth estimation and scene parsing. In *CVPR*, pages 675–684, 2018. 3
- [58] Zizheng Yan, Jiapeng Zhou, Fanpeng Meng, Yushuang Wu, Lingteng Qiu, Zisheng Ye, Shuguang Cui, Guanying Chen, and Xiaoguang Han. Dreamdissector: Learning disentangled text-to-3d generation from 2d diffusion priors. In *ECCV*, 2024. 3
- [59] Lihe Yang, Bingyi Kang, Zilong Huang, Xiaogang Xu, Jiashi Feng, and Hengshuang Zhao. Depth anything: Unleashing

- the power of large-scale unlabeled data. In *CVPR*, 2024. [2](#), [3](#)
- [60] Lihe Yang, Bingyi Kang, Zilong Huang, Zhen Zhao, Xiaogang Xu, Jiashi Feng, and Hengshuang Zhao. Depth anything v2. *arXiv:2406.09414*, 2024. [2](#), [3](#), [5](#), [6](#), [7](#), [9](#)
- [61] Lvmin Zhang, Anyi Rao, and Maneesh Agrawala. Adding conditional control to text-to-image diffusion models. In *ICCV*, 2023. [3](#)
- [62] Richard Zhang, Phillip Isola, Alexei A Efros, Eli Shechtman, and Oliver Wang. The unreasonable effectiveness of deep features as a perceptual metric. In *Proceedings of the IEEE conference on computer vision and pattern recognition*, pages 586–595, 2018. [4](#)
- [63] Zhenyu Zhang, Zhen Cui, Chunyan Xu, Yan Yan, Nicu Sebe, and Jian Yang. Pattern-affinitive propagation across depth, surface normal and semantic segmentation. In *CVPR*, pages 4106–4115, 2019. [3](#)